Thermal Science and Engineering Progress 75 (2026) 104738

Contents lists available at ScienceDirect

Thermal Science and Engineering Progress

journal homepage: www.sciencedirect.com/journal/thermal-science-and-engineering-progress

Thermal interface materials for high-power LED packaging: advances, reliability and design guidelines

Armin Rahmati Darvazi [a,1,*], Alireza Eslami Majd [b,1,*], Nduka Nnamdi Ekere [b], Jin Wang [b]

[a] Faculty of Technology and Engineering (East of Guilan), University of Guilan, Rudsar, Iran
[b] School of Engineering and Built Environment, Liverpool John Moores University, Byrom Street, Liverpool L3 3AF, United Kingdom

ARTICLE INFO

Keywords:
Thermal interface material (TIM)
High-PowerLEDs
Interfacial thermal resistance
Bond-line thickness
Polymer–ceramic nanocomposites
Boron nitride nanotubes

ABSTRACT

Efficient thermal management remains a major constraint in high-power light-emitting diodes (LEDs), where most input electrical power is dissipated as heat, elevating junction temperature and accelerating lumen depreciation and package degradation. This review examines thermal interface materials (TIMs) used in LED packages and modules, organised into four hierarchical families: conventional conformable TIMs, bonded metallic interfaces, engineered composite systems, and architecture-driven or emerging concepts. Representative materials within these families, including greases, gels, pads, solders, phase-change materials, sintered Ag/Cu joints, transient liquid phase sintering systems, liquid–metal hybrids, polymer–ceramic nanocomposites, and nano-architected interfaces, are critically analysed.

Particular attention is given to the coupled roles of through-plane thermal conductivity, bond-line thickness, and interfacial contact resistance, which together determine the effective thermal resistance of TIM layers and the resulting LED junction temperature. Comparative tables and a quantitative design map relate material properties to LED-level performance and reliability considerations, including pump-out, voiding, corrosion, and thermo-mechanical fatigue. Finally, a conceptual roadmap is presented for an electrically insulating TIM based on aligned boron nitride nanotube/nanosheet–epoxy architectures, and a simplified one-dimensional thermal stack analysis illustrates the junction temperature reduction achievable when effective total thermal resistance is minimised at sub-100 μm bond lines.

1. Introduction

The global shift toward energy-efficient and sustainable lighting has accelerated the adoption of solid-state lighting technologies, particularly light-emitting diodes (LEDs) [1,2]. LEDs offer substantial advantages including lower power consumption, longer lifetimes, compact design, and enhanced durability compared to traditional light sources [3,4]. However, thermal management remains a critical challenge in high-power (HP) LEDs. Recent studies indicate that 60–85 % of the input electrical power in LEDs is dissipated as heat due to non-radiative losses [5]. If not efficiently removed, this heat leads to elevated junction temperature (T_j), reduced efficiency, spectral instability, and accelerated degradation mechanisms [6–15].

Driven by increasing chip power density and miniaturisation trends, interfacial thermal resistance (ITR) within HP LED packages has become a dominant factor governing T_j, optical stability, and long-term reliability. Consequently, there is strong industrial and academic interest in thermal interface materials (TIMs) capable of delivering low bond-line thickness (BLT), stable interfacial contact during ageing, and electrical insulation where required. Accordingly, the development of TIM technologies has expanded from conventional formulations such as greases, gels, adhesives, pads, and phase-change materials (PCMs) toward metallic, composite, and nano-architected systems designed to achieve high through-plane thermal conductivity ($k_\perp$) with mechanical compliance at sub-100 μm bond lines.

1.1. Scope and positioning of this review

Existing reviews have addresses either LED thermal management at package and system levels, or TIMs for general electronics applications [16–20]. In contrast, the present review focuses specifically on *TIMs used in HP LED packaging*, treating them as integral elements of a coupled thermo-mechanical reliability problem rather than as isolated bulk

* Corresponding authors.
E-mail addresses: Armrh@guilan.ac.ir (A. Rahmati Darvazi), A.Eslamimajd@ljmu.ac.uk (A. Eslami Majd).
[1] These authors contributed equally and share first authorship.

https://doi.org/10.1016/j.tsep.2026.104738
Received 27 November 2025; Received in revised form 24 April 2026; Accepted 11 May 2026
Available online 14 May 2026

Nomenclature

Symbol/Abbreviation	*Definition*
°C	Degrees Celsius
A	Pre-exponential factor (Arrhenius)
Ag	Silver
Al_2O_3	Aluminium Oxide (Alumina)
AlN	Aluminium Nitride
ASTM D5470	Standard test for thermal transmission of TIMs
BLT	Bond-Line Thickness
BN	Boron Nitride
BNNS	Boron Nitride Nanosheet
BNNT	Boron Nitride Nanotube
CAGR	Compound Annual Growth Rate
CNT	Carbon Nanotube
CTE	Coefficient of Thermal Expansion
Cu	Copper
DAA	Die-Attach Adhesive
DIW	Direct Ink Writing
EG	Expanded Graphite
Ea	Activation Energy (Arrhenius)
f	Failure Rate (Arrhenius)
GaN	Gallium Nitride
GNP/GNs	Graphene Nanoplatelet/Graphene Nanosheet
HDPE	High-Density Polyethylene
HP LED	High-Power Light-Emitting Diode
h-BN	Hexagonal Boron Nitride
ITR	Interfacial Thermal Resistance
JESD51-14	Standard for LED junction-to-case thermal resistance measurement
k_B	Boltzmann's Constant
k⊥	Through-plane Thermal Conductivity
LED	Light-Emitting Diode
LM	Liquid Metal
LINC	Liquid-Infused Nanostructured Composite
MCPCB	Metal-Core Printed Circuit Board
$mm^2 \cdot K \cdot W^{-1}$	Unit of areal thermal resistance
MWNT/SWNT	Multi-Walled/Single-Walled Carbon Nanotube
Ni	Nickel
PCTIM	Phase Change Thermal Interface Material
PCM	Phase Change Material
PDMS	Polydimethylsiloxane
PET/PVC	Polyethylene Terephthalate/Polyvinyl Chloride
PNC	Polymer Nanocomposite
PPS	Polyphenylene Sulphide
Q	Total Steady-state Heat Dissipation
R_C	Thermal Contact Resistance
R_{TIM}	Effective Total Thermal Resistance of TIM
R_{Total}	Total Thermal Resistance of the LED Package
R″	Areal Thermal Resistance
RC (material)	Regenerated Cellulose
SiC	Silicon Carbide
T	Temperature (Arrhenius)
T-CNF	TEMPO-oxidised Nanofibre Cellulose
TC	Thermal Conductivity
TCA	Thermally Conductive Adhesive
TiT_j	TitaniumJunction Temperature
TiC/WC	Titanium Carbide/Tungsten Carbide
TIM	Thermal Interface Material
TIM1	Die-attach thermal interface layer between the LED chip and the submount or package substrate
TIM2	Thermal interface layer between the package heat spreader (or substrate) and the heat sink
TLPS	Transient Liquid Phase Sintering
TR	Thermal Resistance
VOC	Volatile Organic Compound

materials. This focus is motivated by increasing power densities, stricter T_j limits, and the growing dominance of interface-controlled thermal resistance in LED performance.

The main contributions of this review are: (1) an LED–specific TIM selection framework based on T_j, junction-to-case/heat sink thermal resistance, and package-level metrics; (2) a targeted discussion of reliability mechanisms and testing standards relevant to LED packaging; and (3) the introduction of a design map linking BLT, k⊥, and ITR to identify practical performance windows.

The paper is organised to guide the reader from fundamentals to application-oriented design. Heat-flow pathways and performance metrics are introduced in Section 2, followed by reliability considerations and Arrhenius-type behaviour in Section 3. Section 4 presents a structured analysis of TIM materials and architectures for HP LED packaging. Section 5 develops a conceptual design framework, including simplified thermal analysis and reliability considerations, and Section 6 summarises key insights and future research directions.

1.2. Review approach

A structured narrative review methodology was adopted. The main literature survey was conducted using Scopus, Web of Science, IEEE Xplore and Google Scholar for the time window over the period from May 2024 to October 2025, using combinations of "thermal interface material", "TIM", "LED package", "die attach", "high-power LED", "junction temperature", and "thermal resistance" as keywords. Both foundational and recent studies were considered in order to capture historical development and emerging trends. In addition, selected newly published studies available up to April 2026 were incorporated during manuscript revision where they were directly relevant to the discussion. As this work is a narrative synthesis rather than a formal systematic review or *meta*-analysis, no formal risk-of-bias assessment was conducted; instead, the focus is on extracting design-relevant insights for thermal and interfacial engineering in LED packaging.

1.3. Structure of the paper

The remainder of this review is organised as follows. Section 2 outlines heat-flow pathways in LED packages and defines the key performance metrics used to evaluate TIMs. Section 3 discusses reliability considerations relevant to LEDs, including ageing phenomena and Arrhenius-type acceleration concepts. Section 4 presents a structured analysis of TIM material systems and their architectural evolution for HP LED packaging, organised into conventional, bonded metallic, engineered composite, and architecture-driven or emerging concepts, together with comparative performance windows and selection guidance. Section 5 develops a conceptual design and fabrication framework for next-generation electrically insulating TIMs and illustrates, using a simplified one-dimensional (1D) thermal stack analysis, the T_j reduction achievable when the total interfacial thermal resistance of the TIM layer is reduced at sub-100 μm bond lines. This section also discusses degradation mechanisms, qualification considerations, and practical selection guidelines for reliability-aware TIM design in HP LED modules. Finally, Section 6 synthesises the key insights from the review and outlines future research directions for reliable, scalable, and manufacturable TIM solutions in HP LED systems.

2. TIMs and LED thermal management

Effective thermal management is critical for the performance and reliability of LEDs, as excessive T_j degrades luminous efficiency, accelerate aging, and shorten device lifetime. TIMs play a central role in this process by minimising interfacial gaps between mating surfaces, thereby reducing thermal contact resistance (R_C) and enabling efficient heat transfer from the LED junction to the heat sink. TIMs replace air within microscopic surface asperities (air TC ≈ 0.026 $W{\cdot}m^{-1}{\cdot}K^{-1}$) with materials of higher TC, thereby lowering ITR, and improving heat dissipation to the ambient environment.

In HP LEDs, the thermal budget is often dominated by a limited number of series resistances: the die-attach layer, the substrate or heat spreader, and the spreader-to-heat-sink interface.

Fig. 1(a) and (b) illustrate the application of TIMs in a typical LED assembly, highlighting two principal thermal interfaces. TIM1 refers to the die-attach layer between the LED chip and the submount or package substrate, where high TC and thermo-mechanical fatigue resistance are critical. TIM2 refers to the package or spreader-to-heat-sink interface, where conformability and low contact resistance under limited clamping pressure are typically dominant [21–29].

Fig. 1(c) illustrates the presence of microscopic gaps between mating layers and the function of TIMs in filling these voids. Soft materials such as greases, gels, adhesives, and PCMs conform easily to surface irregularities, whereas hard materials may offer mechanical robustness but risk incomplete gap filling and elevated interfacial resistance.

From a thermal-resistance perspective, achieving low R_{TIM} requires more than selecting a material with high bulk TC. The effective interfacial resistance depends on the combined influence of k⊥, BLT, and the real contact area established under the available clamping pressure. As illustrated conceptually in Fig. 1, a high-k material applied at excessive thickness may produce higher TR than a moderate-k material applied as a thin, well-conformed layer. Consequently, co-optimisation of k⊥, BLT, and interfacial contact behaviour is essential for reducing total interfacial resistance in LED modules [21,30–34].

As chip power densities increase and packages become more compact, interface-level resistance increasingly governs T_j, optical stability, and long-term reliability. Therefore, TIM selection in LED systems must consider not only TC but also electrical insulation requirements, thermo-mechanical durability, ageing behaviour, and compatibility with LED packaging architectures [18,35,36]. Recent studies further emphasise the importance of T_j control and phase-change thresholds in maintaining stable performance under cyclic loading conditions [37]. These reliability considerations are discussed in detail in Section 3.

3. Important factors for TIM

Selecting an efficient and reliable TIM for heat sink-based cooling systems requires careful consideration of several key factors, as summarised in Fig. 2.

3.1. Thermal conductivity

The bulk TC of a TIM determines its ability to transfer heat through the material. Since TIMs function as a thermal bridge in LED assemblies, high TC is essential for effective heat dissipation [38,39]. Composite-based TIMs, particularly polymer nanocomposites (PNCs), enhance heat transfer by incorporating high-TC filler, while the polymer matrix fills surface gapsasperities to improve contact [40]. Depending on mechanical and curing behaviour, PNC-based TIMs are generally classified into hard systems (e.g., curable composites, metallic/solder interfaces) and soft systems (e.g., greases and gels) [41]. Representative TC values for TIMs employed in LED packaging are summarised in Table 2 (Section 4).

TC is commonly measured using techniques are utilized such as transient plane source (TPS) method, laser flash analysis (LFA), and 3ω method, with the selection depending on material geometry and required accuracy [42,43]. In LED applications, heat flow is predominantly perpendicular to the interface; therefore, k⊥ is more critical than in-plane TC. Consequently, the orientation and dispersion of nanofillers within composite TIMs strongly influence k⊥ and thus overall interface performance [44].

3.2. Electrical conductivity

Although TIMs primarily provide a thermal pathway, they may also serve secondary roles such as electrical insulation or mechanical attachment depending on the application. TIMs are generally categorised as electrically insulating or conductive [45]. In LED modules, conductive TIMs may enable undesired current leakage between the LED chip and the heat sink, potentially compromising safety and long-term stability [41,46–48]. Consequently, electrically insulating composite TIMs are commonly preferred. Polymer matrices such as epoxy, polystyrene, polyethylene, and polyvinyl alcohol combined with nonconductive fillers provide both electrical insulation and enhanced thermal transport [49–52]. For example, incorporation of boron nitride (BN) nanoparticles, nanosheets, or nanotubes into epoxy/alumina (Al_2O_3) composites significantly improves insulation while maintaining favorable thermal performance [47,53–55]. These composite systems therefore support thermal management while enhancing electrical reliability and package stability [56,57]. Their ease of processing and cost-effectiveness further support widespread application in LED systems [58].

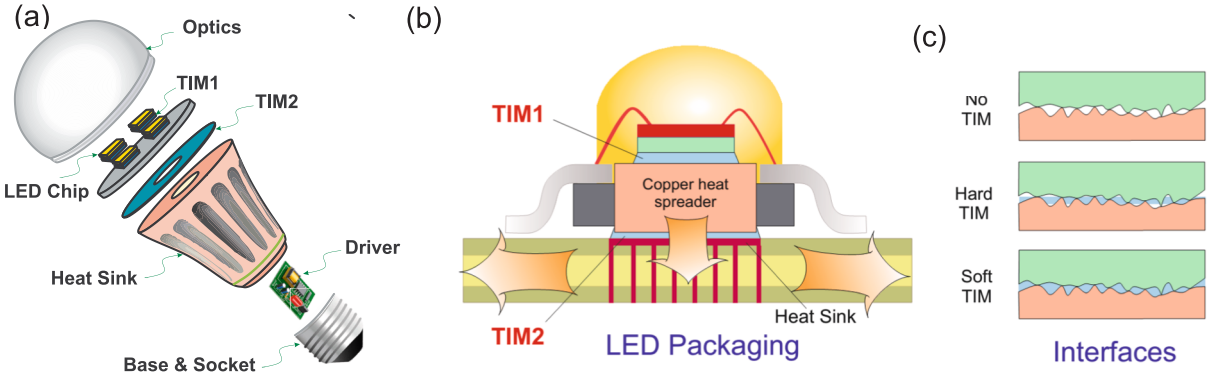

Fig. 1. (a) 3D view of a LED lamp showing the placement of TIMs between mating layers. (b) Cross-section (2D general view) of a typical LED assembly. (c) Interfacial gaps without filler, with a hard filler, and with a soft filler.

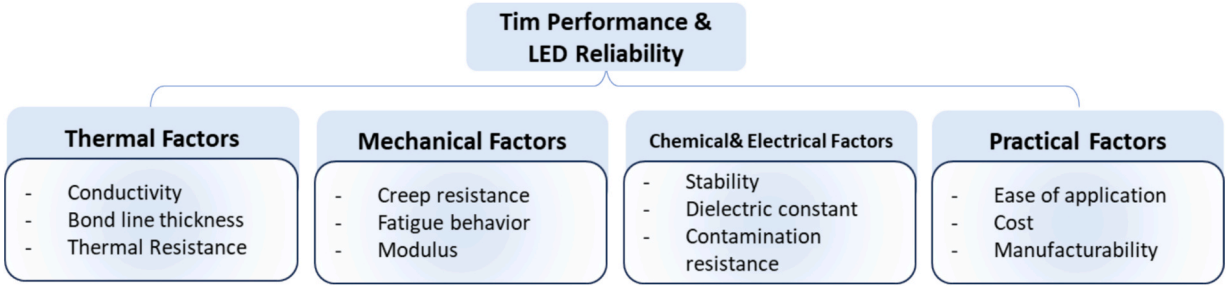

Fig. 2. Key factors and criteria guiding TIM selection for heat sink-based cooling.

3.3. Thermal resistance (TR)

TR quantifies resistance to heat transfer across a material or interface. While TC is an intrinsic material property, the effective TR of a TIM depends on its intrinsic TC, BLT, and R_C, which is influenced by surface roughness, flatness, clamping pressure, and compressive modulus [21,59]. The effective total thermal resistance of TIM (R_{TIM}) can be theoretically expressed as equation (1).

$$R_{TIM} = R_{bulk} + R_{c1} + R_{c2}, R_{bulk} = \frac{BLT}{k_{TIM}} \quad (1)$$

where R_{c1} and R_{c2} are the R_C at the two interfaces, k_{TIM} is the TC of TIM, BLT is the mean bond line thickness (see Fig. 3). High-performance TIMs therefore require low BLT, high TC, and minimal R_C [31–33]. Reducing R_{TIM} directly enhances the heat transfer and overall LED package performance [30].

Because the conductive (bulk) component of ITR is governed by the ratio $BLT/k_{\perp}$, it is useful to represent this relationship graphically. Fig. 4 therefore presents a design map linking BLT and $k_{\perp}$ to the resulting areal bulk thermal resistance, R''_{bulk}, providing a first-order framework for identifying acceptable areal bulk thermal resistance, R''_{TIM}, windows in HP LED packages.

Several practical strategies can reduce TR of a TIM. These include decreasing the BLT, selecting materials with higher TC, and minimising R_C through surface smoothing and controlled clamping pressure. Increased pressure enhances real contact area and reduces gap length, allowing the TIM to conform more effectively to surface asperities [60]. For soft TIMs, compression further reduces BLT and R_{TIM} [21,61]. Employing thinner TIMs simultaneously reduces material consumption and improves thermal performance by directly lowering BLT [62].

Recent developments highlight engineered approaches that target simultaneous reduction of BLT and R_C. For example, a boron nitride nanotube (BNNT)-modified (Aluminium Nitride/Aluminium Oxide) AlN/Al_2O_3–PDMS composites achieved reduced TR through improved filler dispersion and interfacial adhesion [63]. Surface functionalisation of graphite–copper interfaces significantly decreased R_C, emphasising the importance of interface modification [64]. Self-adaptive liquid–metal–epoxy composites that cure in situ demonstrated improved gap filling and reduced void formation under pressure. This behavior minimises BLT and reduces interfacial voids, leading to a lower overall TR [65]. Rheology-based predictive models have further enabled optimization of BLT through viscosity control at high filler loading [66]. Ultrathin BN/T-CNF/PVA composite films have also demonstrated enhanced TC and mechanical robustness, supporting their suitability for compact electronic systems [67].

These representative strategies, summarised in Table 1, illustrate the shift toward engineered TIM systems that integrate high TC, reduced BLT, and controlled interfacial contact resistance to improve LED thermal management.

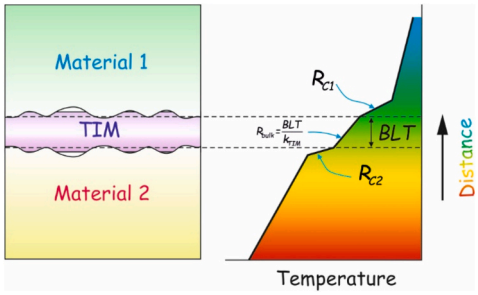

Fig. 3. Schematic illustration of a TIM filling the interfacial gap between two surfaces to minimise R_C and facilitate heat conduction.

3.4. Junction temperature

The junction temperature, T_j, strongly influences both the optical performance and the lifetime of an LED chip [30,68]. Reliability studies show that LED failure rates increase exponentially with T_j. This behaviour is commonly described using an Arrhenius-type relation for thermally activated degradation processes [69,70]:

$$f = A\exp\left(-\frac{E_a}{k_B T_j}\right) \quad (2)$$

where f is the failure rate, A is the pre-exponential factor (assumed temperature-independent for a given failure mechanism), E_a is the activation energy of the dominant degradation process, k_B is the Boltzmann constant, and T_j is the junction temperature in Kelvin. This formulation assumes a single dominant thermally activated failure mechanism and is widely used to describe temperature-accelerated degradation in LED systems [71,72].

To quantify this sensitivity in a form directly relevant to LED operating conditions, Fig. 5 presents the Arrhenius acceleration factor relative to a reference T_j of 85 °C for representative activation energies typical of LED package and interfacial degradation processes. The logarithmic scale highlights the rapid increase in failure rate as T_j rises beyond the recommended operating window. Elevated T_j also degrades LED optical performance. A 10 °C rise in T_j has been reported to reduce optical output power by approximately 5 %, decrease forward voltage by ~20 mV, and shift the dominant wavelength by ~2 nm [73,74].

The relationship between T_j and LED lifetime is illustrated in Fig. 6, based on experimental data for a HP LED operated at maximum continuous forward current. Lifetime decreases significantly once the T_j exceeds approximately 120 °C [75,76]. Long-term studies confirm accelerated degradation at elevated temperatures; for example, Caria et al. [77] observed lens darkening, silicone cracking, and solder fatigue in HP LEDs stressed above 120 °C.

For reliable operation, T_j should remain well below the absolute maximum rating (typically 150 °C) and ideally ≤85–105 °C. Temperatures approaching 120–125 °C accelerate package-level degradation and substantially shorten operational lifetime [13,77–80]. Consequently, effective thermal management is essential for maintaining T_j within safe limits and preventing premature lifetime reduction and catastrophic

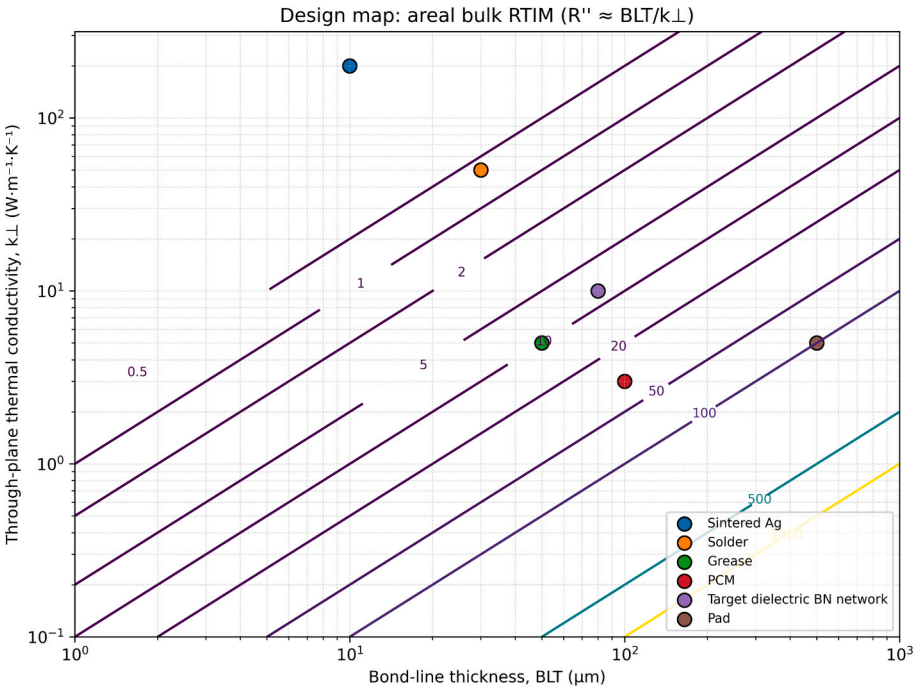

Fig. 4. Design map showing the relationship between BLT and $k_{\perp}$ for the areal bulk thermal resistance ($R''_{bulk} \approx \mathrm{BLT}/k_{\perp}$, expressed in $\mathrm{mm^2{\cdot}K{\cdot}W^{-1}}$). Representative positions of major TIM systems (sintered Ag, solder, grease, PCM, pad and a target dielectric BN network) are indicated for comparison.

Table 1
Recent advances in TIM strategies for reducing TR.

TIM system	Approach	Technical Strategy	BLT/$\mathbf{R_C}$ Effect	Thermal Properties	Ref.
BNNT–PDMS with AlN/Al_2O_3	Filler modification with BNNTs	*Filler Engineering*	Achieves ultralow BLT via improved filler–matrix adhesion	Enhanced through-plane heat conduction	[63]
Graphite–Copper (Treated Interface)	Surface functionalization of copper	*Interface Engineering*	R_C *reduced* from 87.96 to 20.26 $\mathrm{mm^2{\cdot}K.W^{-1}}$; 7 °C lower operating temperature	Improved interfacial thermal conductance	[64]
In-situ Cured LM–Epoxy Composite	Pressure-induced adaptive curing	*Self-Adaptive Composite*	BLT minimised (~2.19 $\mathrm{mm^2{\cdot}K.W^{-1}}$); cured composite prevents LM leakage	kTIM up to 10.05 $\mathrm{W{\cdot}m^{-1}{\cdot}K^{-1}}$; stable pad form; strong adhesion (0.497 MPa)	[65]
Polymeric TIMs (Rheology-Based Design)	Predictive modeling using MDTS model	*Rheology-Guided Design*	Enables BLT estimation across filler loads; captures filler–matrix interactions	Accurate BLT prediction under pressure; design optimisation	[66]
Nanosized BN/PVA/T-CNF Ultrathin Film	Nanoscale BN exfoliation + T-CNF reinforcement	*Ultrathin Hybrid Film*	Ultrathin (~50 μm) with strong filler dispersion and low R_C	In-plane: 11.13 $\mathrm{W{\cdot}m^{-1}{\cdot}K^{-1}}$; Through-plane: 1.22 $\mathrm{W{\cdot}m^{-1}{\cdot}K^{-1}}$; flexible and robust	[67]

failure.

Accurate determination of T_j is therefore critical. Indirect include forward-voltage monitoring, spectral shift methods, Raman spectroscopy, and liquid–crystal thermography [81,82]. More advanced approaches such as transient thermal analysis and micro-Raman thermography provide improved spatial and temporal resolution [83].

T_j may also be estimated using the total thermal resistance of the LED package as:

$$T_j = R_{Total} \times Q + T_a \tag{3}$$

where Q is the total steady-state heat dissipation and T_a is the ambient temperature. The total thermal resistance R_{Total}, is obtained by summing the TRs of all package components along the heat-flow path from the junction to the ambient. This relationship highlights that any reduction in interfacial resistance, including that of the TIM layer, directly lowers R_{Total} and therefore reduces the resulting T_j under a given thermal load.

Fig. 7 presents an example R–C curve (thermal resistance versus thermal capacity) for a representative LED package, including the chip, solder joint, TIM, heat spreader, heat sink, and ambient environment [84].

Table 2 further summarises representative studies reporting LED-level thermal metrics associated with different TIM implementations, thereby illustrating how improvements at the interface level translate into measurable reductions in overall thermal resistance and T_j.

3.5. Phase-change temperature

The phase-change temperature defines the transitions at which a phase change TIM softens or melts, enhanced conformability and improved interfacial contact. In HP LED packages, this transition should occur within the normal operating T_j so that the material softens during operation and fills interfacial asperities, thereby reducing contact thermal resistance. However, the transition temperature must remain sufficiently above expected non-operating conditions, such as storage or transportation temperatures to prevent premature softening, leakage, or material migration.

This design constraint requires careful matching of the phase-transition temperature to the intended LED operating window. Excessively low transition temperatures may compromise mechanical stability and lead to pump-out or drip-related failures, whereas excessively high transition temperatures limit the material's ability to conform under realistic operating conditions. The use of materials with controlled viscosity and shape stability can mitigate these risks when

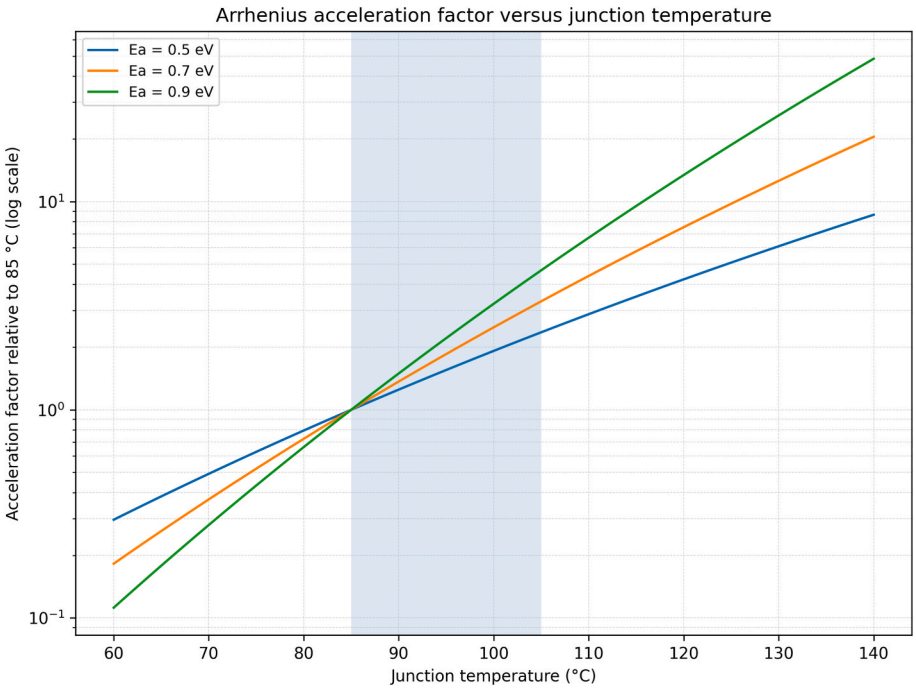

Fig. 5. Arrhenius acceleration factor of failure rate as a function of T_j, normalised to 85 °C.

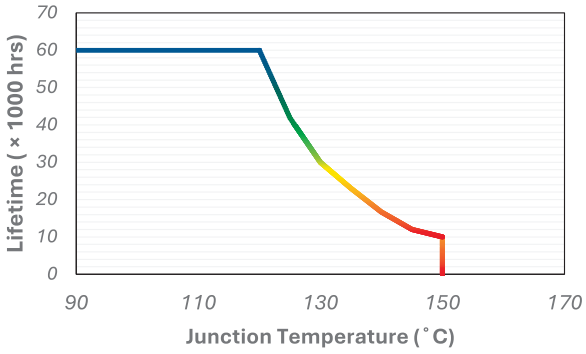

Fig. 6. Relationship between T_j and the lifetime of an HP LED at maximum continuous forward current (representative trend), adapted from [76].

properly selected for the application temperature range [21,88]. For example, phase-change TIMs with transition temperatures in the range of 53.84– 61.37 °C [88], 66.8–73.2 °C [89], and approximately 77 °C [90], have been reported to provide effective thermal management while maintaining stability under non-operating conditions. Therefore, appropriate selection of the phase-change temperature is essential for maintaining low interfacial resistance, ensuring thermal reliability, and preserving long-term optical performance in LED modules.

3.6. Other factors

In addition to TC and ITR, several secondary properties critically influence the long-term performance of TIMs in LED packages. Mechanical properties, including creep resistance viscoelastic stability, and thermo-mechanical fatigue behavior, directly affect bond-line stability during thermal cycling. Chemical stability is equally important, particularly with respect to oxidation, hydrolysis, and compatibility with metallised substrates. Electrical characteristics such as dielectric strength and dielectric constant must also be considered in electrically insulating LED architectures. Furthermore, spreading behaviour, wetting characteristics, and resistance to contamination influence interfacial integrity and manufacturing reproducibility. From an industrial perspective, processability, dispensing behaviour, curing requirements, and overall cost strongly impact scalability and commercial viability [21,91,92].

Therefore, optimal TIM selection in LED systems requires a multi-criteria approach that balances thermal, mechanical, electrical, chemical, and manufacturing considerations rather than prioritising bulk TC alone. In this context, an ideal TIM must combine high TC, thermal stability, electrical insulation (where required), corrosion resistance, mechanical compliance, and processability [39,93].

4. Material systems and architecture evolution of TIMs for HP LEDs

This section reviews emerging TIM strategies for HP LED applications, including advanced composites, phase-change materials, liquid metals, and two-dimensional material-based architectures. These approaches aim to reduce interfacial thermal resistance while enabling improved reliability, conformability, and multifunctional performance.

TIM technologies for HP LED packaging have evolved through a clear materials and interface progression driven by increasing heat flux, stricter reliability requirements, and packaging constraints. Early implementations relied mainly on soft greases and gels, which offered low contact resistance and simple processing but were limited by pump-out, dry-out, and long-term stability concerns [51,94–96]. As thermal demands increased, ceramic-filled polymer TIMs based on fillers such as BN, Al_2O_3, and AlN became more widely adopted because they provided a useful balance between TC, dielectric performance, and manufacturability, although often with relatively high BLT and limited $k_{\perp}$ [48,51,52,97,98]. This was followed by bonded metallic TIMs, including solder, sintered Ag/Cu, and TLPS systems, which enabled thinner bond lines and lower interfacial resistance, particularly for TIM1 in HP LED packages [22,27–29,99]. More recently, the field has shifted towards architecture-driven and adaptive TIM concepts, including aligned filler networks, nano-architected contacts, MXene-based systems, bio-inspired interfaces, and additively manufactured or switchable TIM architectures, all of which aim to co-optimise $k_{\perp}$, BLT, interfacial contact,

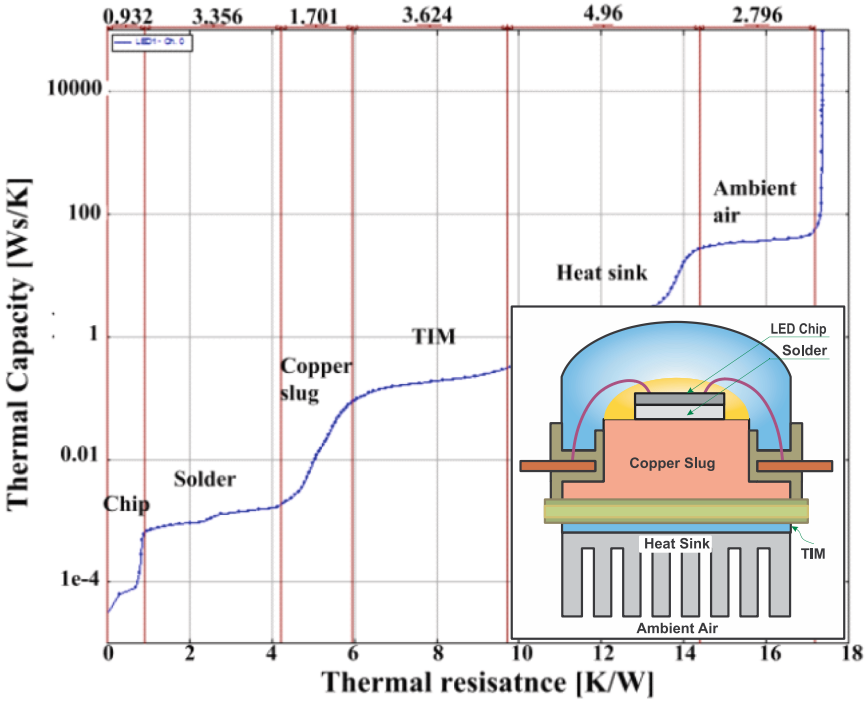

Fig. 7. TR via thermal capacity (thermal R-C curve) of a typical LED package, adopted from [84].

Table 2
Representative TIM studies reporting LED-level thermal metrics (R_{Total} and/or ΔT_j,). Note: Values are as reported by the cited studies and are not directly comparable unless test conditions are matched.

LED context	TIM/interface	Conditions	Reported LED-level outcome	Study/ ref.
'Big-chip' projector LEDs; die attach (TIM1)	Ag-epoxy vs sintered nano-Ag	Several die sizes; R_{Total} measured via wavelength shift	Example (PT39CX): R_{Total} 1.86 → 0.97 K/W (Δ = 0.89 K/W);	[22]
HP LED with AlN substrate; bonding layer ageing	Nano-Ag vs Au80Sn20 vs SAC305 (TIM1)	350 mA; ageing at 100 °C up to 500 h	Before ageing: R_{Total} was 4.82 for (nano-Ag), 7.84 (AuSn), 8.75 K/W (SAC). After 500 h ageing: 9.54, 13.98, 16.59 K/W, respectively; nano-Ag shows least increase (+1.5 % in bonding-layer Rth).	[85]
LED package cooling using nano-pastes (TIM2)	Carbon nanotube (CNT) paste; graphene paste	Reported under comparable operating conditions	LED chip temperature reduced by 7.5 °C (CNT) and 5.5 °C (graphene) relative to baseline.	[86]
10 W power LED; heat-sink interface	Graphene–epoxy composite TIM (TIM2)	Case study at 10 W	Simulated T_j decreases from 72 °C to 67 °C after TIM insertion (Δ T_j ≈ 5 °C).	[87]

and reliability under realistic operating conditions [18,37,100–106].

Based on this evolution, TIM materials relevant to LED packaging (as illustrated in Fig. 8(a)) can be categorised as follows: (i) conventional bulk TIMs, (ii) bonded metallic TIMs, (iii) engineered composite TIMs, and (iv) architecture-driven and emerging TIM concepts. Table 3 summarises representative performance windows of major TIM systems in terms of k⊥, BLT, R_{TIM}, dielectric behaviour, and typical LED interface (TIM1 or TIM2). Table 4 further complements this by outlining key functional characteristics, dominant reliability risks, and manufacturing considerations for each system listed in Table 3. Fig. 9 provides a qualitative radar comparison to assist material selection.

Historically, as illustrated in Fig. 8(b), TIM development in LED packaging has evolved in response to increasing chip power density and stricter thermal constraints. Early modules relied mainly on soft greases and gels to minimise interfacial thermal resistance at modest heat flux, but pump-out and ageing limited long-term reliability. With rising power density and insulation demands, ceramic-filled polymer systems became more prevalent due to their dielectric strength, compliance, and manufacturing compatibility. For die-attach applications, conventional solder and Ag-epoxy were increasingly replaced by sintered Ag/Cu and transient liquid-phase sintered (TLPS) joints to enable thinner bond lines and improved high-temperature stability.

More recently, advances in nanomaterials and interface engineering have enabled composite systems with engineered filler alignment, hierarchical networks, and nano-architected contacts that co-optimise k⊥, BLT, R_c, and thermo-mechanical reliability under thermal cycling [21–29,94,95,100,101,107–113]. The expanding adoption of high-brightness LEDs in automotive, display, general lighting, and smart systems has further intensified research on polymer composites, PCMs, and hybrid organic systems capable of combining high TC with mechanical and chemical stability under demanding operating conditions [114,115]. In parallel, the integration of wide-bandgap semiconductor platforms such as gallium nitride (GaN) and silicon carbide (SiC), together with advanced packaging technologies, has resulted in higher heat flux densities and stricter ITR constraints, thereby defining new performance targets for next-generation TIM development [116,117].

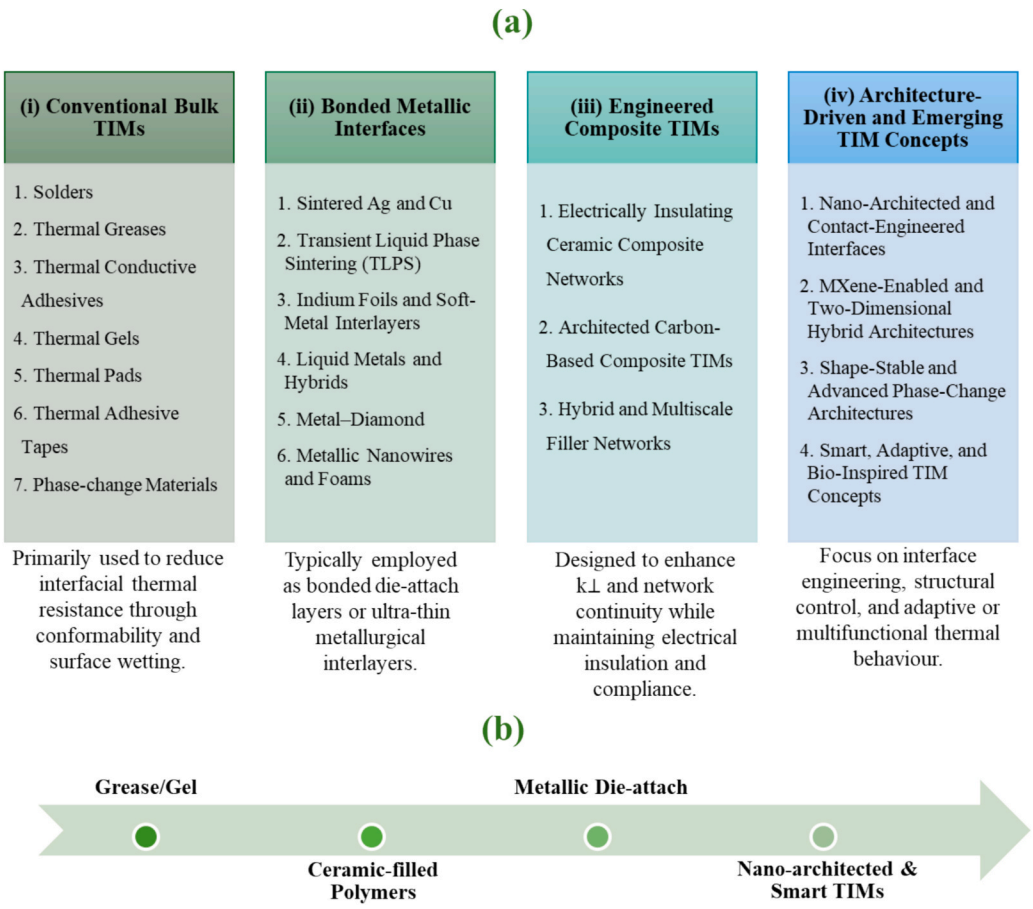

Fig. 8. (a) Hierarchical classification of TIM families for HP LED packaging. (b) Evolution of TIM concepts from conformable bulk systems to bonded, composite, and architecture-driven designs under increasing thermal and reliability demands.

Table 3
Representative performance ranges of major TIM systems used in HP LED packages. Reported values represent indicative ranges and may vary with pressure, surface finish, and processing conditions [21,94,95,118].

Representative TIM Systems	k⊥ ($W{\cdot}m^{-1}{\cdot}K^{-1}$)	BLT (μm)	Areal R_{TIM} ($mm^2{\cdot}K{\cdot}W^{-1}$)	Dielectric	LED interface
Greases	0.4–15	20–100	1–10	Usually yes*	TIM2
Thermal Gels	2–12	100–500	3–20	Yes	TIM2
Pads	0.8–25	200–1000	10–50	Yes	TIM2
Adhesive Tapes (PSA)	0.2–3	50–200	10–50	Yes	TIM2
PCMs	0.7–8.5	50–200	1–15	Yes	TIM2
TCAs/Polymer DAAs	0.5–10 (up to ~ 35)	20–150	2–20	Often yes	TIM1
Solders	20–80	10–50	<1–5	No	TIM1
Sintered Ag/Cu	110–240	5–30	<0.5–2	No	TIM1
TLPS	20–60	10–50	~1–5	No	TIM1
Liquid-Metal TIMs	10–80	<5–50	<1–5	No	TIM2/niche TIM1
	5–40+	50–150	≤2–10	Yes	TIM2/dielectric TIM1

*Some greases contain conductive fillers and may require insulation barriers.

4.1. Conventional bulk TIMs

Conventional TIMs remain widely used in LED packaging due to their process maturity and established reliability. These materials primarily reduce interfacial resistance through conformability or metallurgical bonding at the interface. Fig. 10 shows representative conventional TIM types commonly employed in LED modules.

4.1.1. Solders

Solder-based TIMs, supplied in paste or foil form, are widely used to create a thin, metallurgical bond lines between mating substrates. Unlike polymer-based greases or pads, solder TIM forms a metallic interface that minimises R_C, thereby providing efficient heat conduction across the joint. Their TC typically ranges from 20 to 80 $W{\cdot}m^{-1}{\cdot}K^{-1}$, substantially exceeding that of conventional polymer TIMs (generally <10 $W{\cdot}m^{-1}{\cdot}K^{-1}$), making them particularly suitable for HP LEDs [21,33,121].

Due to their high thermal performance and structural stability, solder TIMs are extensively employed in HP electronics, power modules, and automotive systems operating under sustained thermal loads and environmental stress [99,122]. However, their relatively high elastic modulus compared with semiconductor substrates can generate significant thermo-mechanical stresses during thermal cycling. This stiffness mismatch may lead to interface cracking, fatigue damage, and eventual delamination, compromising long-term package reliability [123,124].

To mitigate stress-induced failures, softer alloys such as indium-

Table 4
Functional characteristics and dominant reliability considerations of major TIM systems in LED packages [33,78,119,120].

Representative TIM systems	Key advantages	Dominant reliability risks	Manufacturing complexity
Greases	Thin BLT; excellent wetting; low cost	Pump-out; bleed/dry-out; contamination	Very low
Thermal gels	Conformable; reduced pump-out after cure	Cure shrinkage; ageing	Low–Moderate
Pads	Easy handling; dielectric isolation	High BLT; creep; compression relaxation	Low
Adhesive tapes	Fast assembly; no curing	Low TC; adhesive creep	Very low
PCMs	Pad handling + grease activation	Leakage; phase instability under cycling	Low–Moderate
TCAs/DAAs	Structural bond + insulation	Voiding; delamination; CTE mismatch	Moderate
Solders	Low R_C; metallurgical joint	CTE fatigue; voiding	Moderate–High
Sintered Ag/Cu	Ultra-low R_C; high-T stability	Process sensitivity; cost	High
TLPS	High-T capability; thin BLT	IMC brittleness	High
Liquid-metal	Ultra-thin BLT; high wetting	Electrical shorting; Ga corrosion	Moderate
Architected composites	Co-optimised k⊥ & BLT; dielectric	Interface ageing; scalability	Emerging

based or low-yield-stress alloys have been investigated. Nevertheless, these systems often exhibit limited thermal fatigue resistance and may be susceptible to void formation during reflow processing [125,126]. In addition, solder-based TIMs require elevated assembly temperatures, which can increase manufacturing complexity and impose compatibility constraints for temperature-sensitive components [127–129].

4.1.2. Thermal grease

Thermal greases (thermal paste TIMs), are widely used in LED packaging due to their ease of application, low cost, and ability to form thin bond lines form that reduces R_{TIM}, typically to values on the order of ~10 $mm^2 \cdot K \cdot W^{-1}$. Their high conformability enables effective filling of surface asperities, improving thermal contact between mating surfaces.

These materials generally consist of thermally conductive fillers such as metals (e.g., silver and copper) or ceramics (e.g., aluminum oxide, zinc oxide, and BN), dispersed within a low TC organic matrix phase (e.g., silicone grease or polymer-based materials). Recent developments include graphene- and carbon-nanotube (CNT)-enhanced greases designed to improve thermal transport. For instance, a graphene-loaded grease (15 wt%) achieved a TC of 13.4 $W \cdot m^{-1} \cdot K^{-1}$, demonstrating effective heat dissipation for LEDs below 50 W [130]. Similarly, incorporation of 0.75 wt% CNTs increased TC by approximately 16 %, resulting in a reported 7.5 °C reduction in LED T_j [86].

Despite their advantages, thermal greases exhibit limitations under elevated temperatures. Their semi-fluid nature may lead to pump-out, phase separation, or bleed-out during thermal cycling, degrading long-term interface stability and reliability [48,96,131,132]. thermal greases exhibit limitations under elevated temperatures. Their semi-fluid nature may lead to pump-out, phase separation, or bleed-out during thermal cycling, degrading long-term interface stability and reliability [94,118].

4.1.3. Thermal conductive adhesives

TCAs are polymer-based TIMs formulated with thermally conductive fillers (e.g., ZnO nanowires, metallic or ceramic particles) dispersed within a polymer matrix. When cured under pressure or fastening, they form a durable bond layer between substrates [133]. Compared to other conventional TIMs, TCAs provide stronger adhesion and improved structural integrity at the interface [33,127]. Unlike gels and greases, TCAs can effectively adhere directly to chip surfaces without overflow issues, while also offering mechanical support between chips and heat sinks. However, TCAs typically exhibit moderate TC and therefore are often engineered high filler loadings to enhance heat conduction and reduce R_C. At elevated temperatures, limitations may arise due to degradation, interfacial delamination, or long-term mechanical instability [61,134,135].

A particularly critical application of TCAs in LED packaging is their use as die attach adhesives (DAAs), where they form the primary thermal and mechanical interface between the chip and submount (Fig. 11). DAAs in HP LEDs include (i) polymer-based TCAs (typically epoxy matrices filled with metallic or ceramic particles), and (ii) semi-sintering or fully sintering metal pastes that form metallic networks upon curing or sintering (see Section 4.2.1). In polymer DAAs, nano- or micro-fillers such as Ag nanoparticles/nanorods or Ni nanochains are incorporated to form percolating thermal pathways that enhance heat transport [136]. Because the die-attach layer lies directly along the principal heat-flow

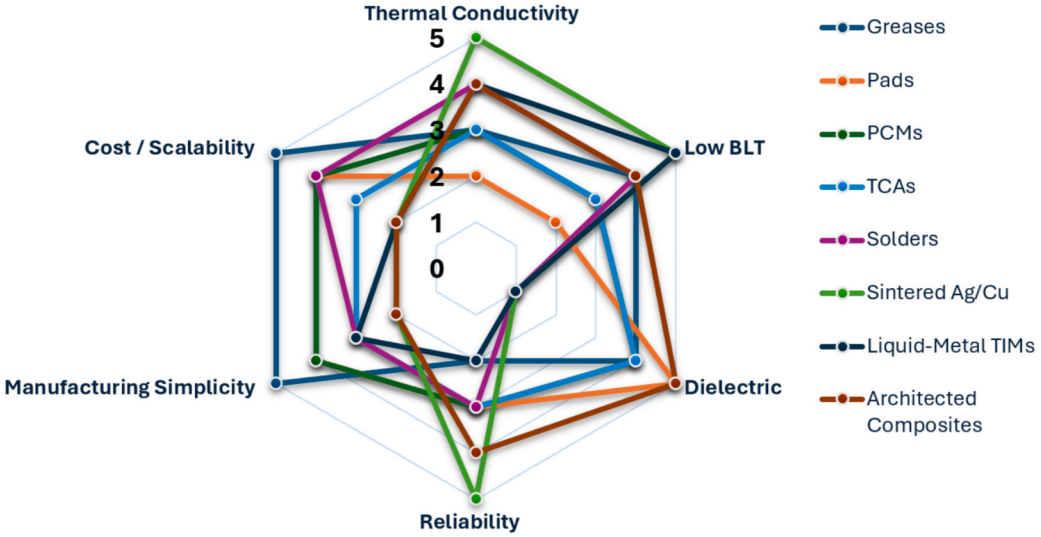

Fig. 9. Qualitative radar comparison of representative TIM systems for HP LEDs (1–5 scale; 5 = best relative performance). Scores reflect relative literature trends and serve as a comparative selection aid alongside Table 3 and Table 4.

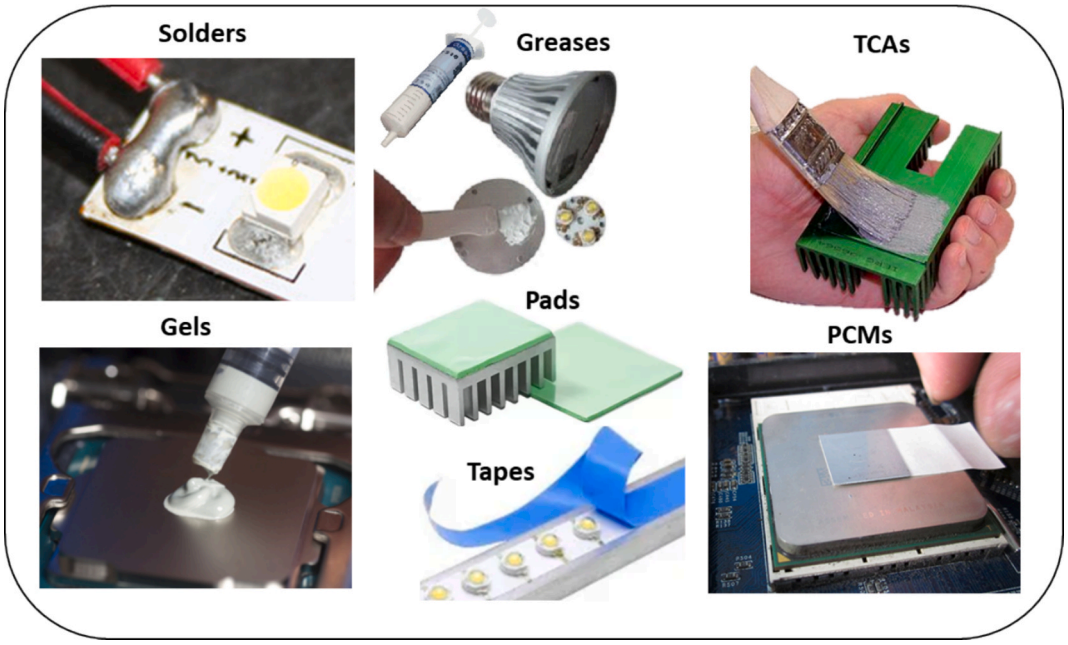

Fig. 10. Conventional TIMs used in LED modules.

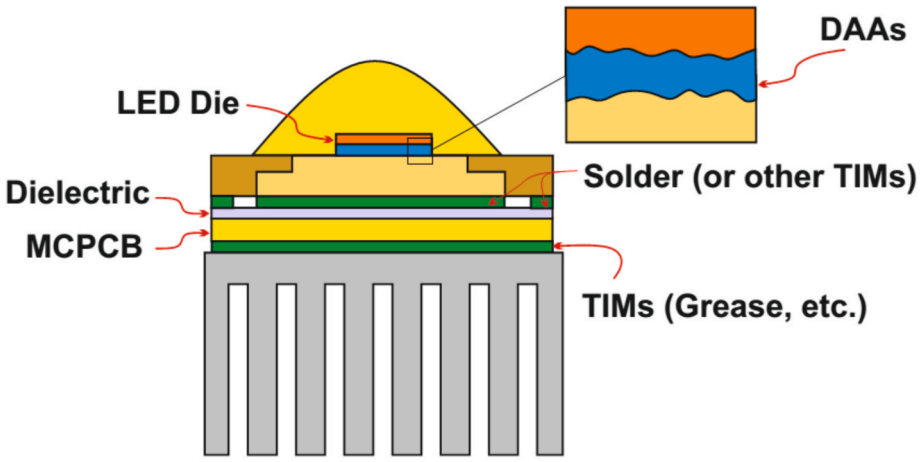

Fig. 11. Cross-sectional view of an LED package using DAA TIM at the LED chip-spreader interface (TIM1) and a solder TIM at the spreader-heat sink interface (TIM2).

path, its thermal resistance is governed by both intrinsic TC and process-dependent parameters such as BLT and voiding [137].

Reported bulk TC values for polymer DAAs are typically 0.5–10 $W{\cdot}m^{-1}{\cdot}K^{-1}$, with optimised systems reaching ~ 20–35 $W{\cdot}m^{-1}{\cdot}K^{-1}$. Semi-sintering Ag DAAs can achieve ≈ 110–165 $W{\cdot}m^{-1}{\cdot}K^{-1}$, while full-sintered Ag exceeds 200–240 $W{\cdot}m^{-1}{\cdot}K^{-1}$ [127,136]. Although DAAs offer strong adhesion and manufacturability, their coefficient of thermal expansion (CTE) is generally mismatched to semiconductor die materials (e.g., epoxy ≫ Si), and stress accommodation relies primarily on adhesive compliance rather than CTE matching. The high cost of Ag-based systems continues to motivate research into Cu-based sintering and alternative cost-effective or electrically insulating DAA chemistries for advanced LED designs [137,138].

4.1.4. Thermal gels

Thermal gels (also referred as putties or dispensable gap fillers) are particle-filled silicon-based composites containing thermally conductive metallic or ceramic fillers dispersed within a polymer matrix. These curable materials exhibit viscoelastic behaviour due to relatively weak bonding between fillers and the matrix, allowing them to combine liquid-like conformability with solid-like structural stability after curing [139,140].

During application, thermal gels flow easily to fill the interfacial gaps (similar to grease), subsequent curing forms a soft, cross-linked polymer network that mitigates pump-out under thermal cycling. However, their relatively low mechanical strength limits their ability to absorb significant thermomechanical stress [141,142].

Thermal gels share similarities with TCAs but are generally softer and provide weaker adhesion between substrates [33]. Their compliance makes them suitable for assemblies containing delicate or geometrically complex components where stress minimisation is critical [143]. In low-power LEDs (typically <50 W), where heat flux is moderate, thermal gels with TC values in the range of ~2–12 $W{\cdot}m^{-1}{\cdot}K^{-1}$ may provide adequate thermal performance.

4.1.5. Thermal pads

Thermal pads (elastomeric pads or gap fillers) are composite TIMs comprising thermally conductive fillers (typically ceramic particles)

dispersed within silicone or other elastomeric matrices [33,95,118]. They are widely used due to of their ease of handling, low cost, and reliable compression behavior during assembly. In addition to the thermal management, thermal pads often provide electrical insulation between the chip and the heat sink, making them suitable for electrically sensitive applications [59,61,144]. They are commonly applied in low-power devices including LEDs, chipsets, and mobile processors [32,118,145,146].

Compared with other TIMs, thermal pads typically exhibit larger BLT values (≈200–1000 μm), which increases their intrinsic areal resistance. Proper conformability requires sufficient clamping pressure, and therefore pad softness plays a critical role in reducing the effective bond line during assembly. Increasing compliance generally requires lowering filler volume fraction; however, this reduces TC. Consequently, the thermal performance of pads is governed by a fundamental trade-off between conductivity and mechanical softness [32,118].

4.1.6. Thermal adhesive tapes

Thermal adhesive tapes, or pressure-sensitive adhesives (PSAs), are used to bond low-power LED chips to spreaders or heat sinks without mechanical fasteners. PSAs are supplied in rolls or as die-cut formats, with adhesive layer coated on both sides of a carrier substrate such as polyethylene terephthalate (PET), polyvinyl chloride (PVC), or silicone rubber. Their key advantages include low cost, rapid assembly, and elimination of post-curing processes. In addition, PSAs can provide electrical insulation between the LED and the heat sink.

However, their relatively low TC (~0.2–3 $W \cdot m^{-1} \cdot K^{-1}$), significantly limits their thermal performance. Reliability may also be compromised by CTE mismatch, surface contamination, adhesive creep under cyclic thermal loading, which can degrade interfacial stability over time [59,134,147–149]. Consequently, PSAs are generally restricted to low-power or low-heat-flux LED applications.

4.1.7. Phase change materials

PCMs combine advantageous features of both thermal greases and pads. A PCM consists of a matrix material with a melting temperature between room temperature and the device operating temperature. his enables pad-like handling at ambient conditions, while softening or melting during operation to form a thin, conformal interfacial layer similar to grease [150,151].

Beyond interfacial conformity, PCMs offer latent heat storage capability, allowing absorption and release of thermal energy during temperature fluctuations [152,153]. Typical matrices include paraffins, polymers, or copolymers, often combined with thermally conductive fillers such as carbon-based nanostructures (nanofibers, nanoplatelets, graphene flakes), metals (Ag, Fe, Au, Cu), metal oxides (Al_2O_3, CuO, MgO, TiO_2), and metallic nanowires [152,154].

Depending on formulation and filler loading, PCMs typically achieve R''_{TIM} on the range of ~1–10 $mm^2 \cdot K \cdot W^{-1}$ [141,155], making them suitable for HP LED interfaces (Fig. 12) [156,157]. However, repeated phase transitions may induce interfacial degradation or chemical interaction at mating surfaces, potentially affecting long-term reliability. Leakage or pump-out can also occur if operating temperatures exceed the designed phase-change range, representing a key limitation

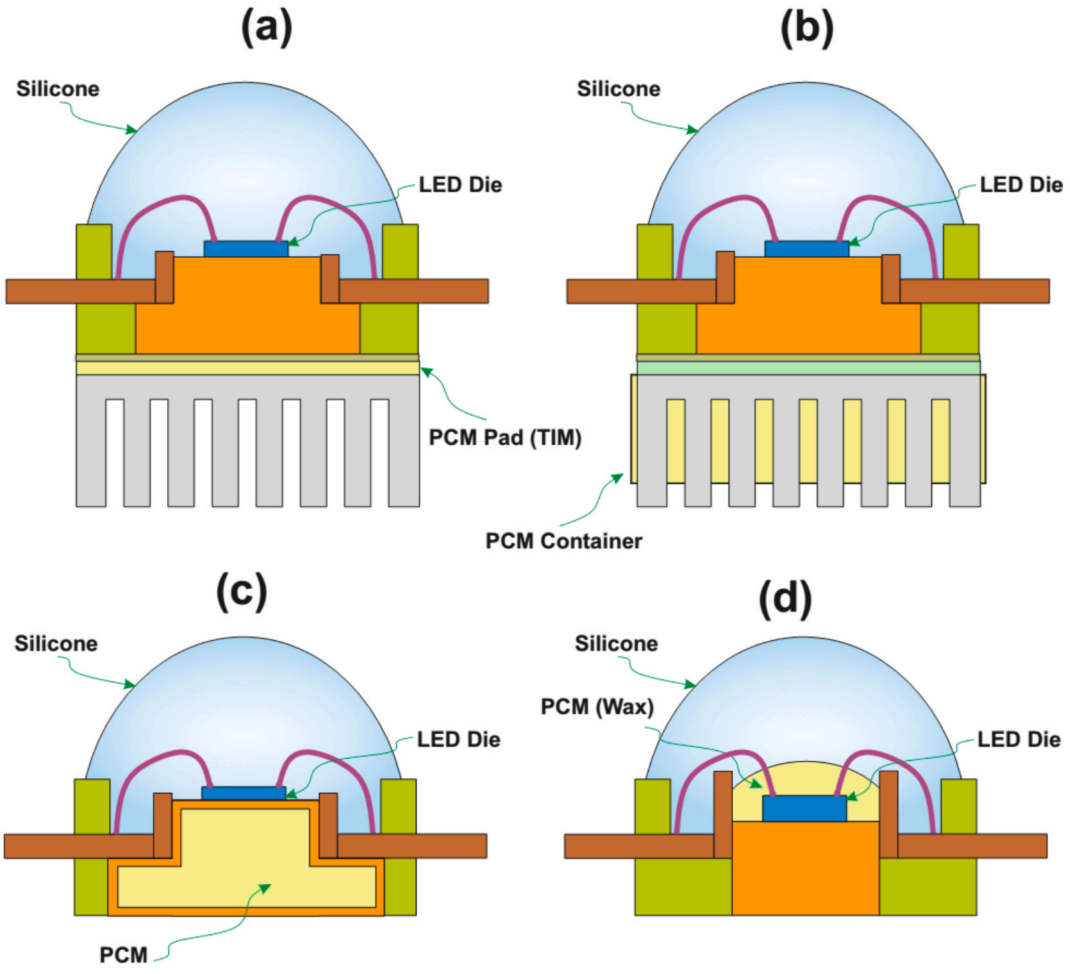

Fig. 12. Representative applications of PCMs in LED systems: (a) used as a TIM exhibiting pad-like handling and grease-like conformity; (b–c) integrated with heat sink–vapor chamber assemblies; and (d) incorporated as part of the encapsulation material.

[120,158].

For LED applications, PCMs are particularly attractive where assembly pressure is limited or where a pad-like handling form is preferred. Once activated, the molten phase reduces R_C and compensate for surface non-flatness. However, LEDs operating in outdoor or enclosed luminaires may experience significant ambient excursions; therefore, the phase-change temperature must remain above the highest expected storage or service temperature to avoid unintended softening, while still low enough to activate during initial burn-in [133,159–164]. Fig. 12 illustrates PCM integration as a TIM, in conjunction with heat sink–vapor chamber assemblies, and as part of encapsulation strategies.

4.2. Bonded metallic TIMs

Bonded metallic TIMs are characterised by heat transport dominated by continuous metallic pathways formed through sintering, liquid-phase interdiffusion, or soft-metal contact rather than polymer-mediated percolation. By minimising porosity, reducing BLT, and improving metallurgical bonding quality, these systems are designed to achieve very low R''_{TIM} under the high heat-flux conditions typical of TIM1 in HP LED packages.

At the LED-package scale, advanced metallic interfaces commonly achieve k⊥ ≥Âf10 $W{\cdot}m^{-1}{\cdot}K^{-1}$ at BLT ≤100 μm and area $lR''_{TIM} \leq 5$ $mm^2{\cdot}K{\cdot}W^{-1}$ under moderate contact pressure, together with improved stability during thermal cycling and high-temperature operation. Contemporary studies emphasise that interfacial quality and microstructural control, rather than nominal bulk conductivity alone, govern performance improvements in these metallic systems [18].

4.2.1. Sintered Ag and Cu

Nanoparticle Ag or Cu pastes densify into porous metallic joints through pressure-assisted (~230 °C, ≥ 10 MPa) or pressure-less (≤250 °C) sintering, forming ultra-thin BLT interfaces with low R''_{TIM}. Joint-scale TC is primarily limited by residual porosity: typically, ~100–200 $W{\cdot}m^{-1}{\cdot}K^{-1}$, with low–porosity Ag routinely >200 $W{\cdot}m^{-1}{\cdot}K^{-1}$; representative values include ~224 $W{\cdot}m^{-1}{\cdot}K^{-1}$ (pressure-less nano-Ag), ~115 $W{\cdot}m^{-1}{\cdot}K^{-1}$ (~10 % porosity), and ~240 $W{\cdot}m^{-1}{\cdot}K^{-1}$ in LED die attach. Pressure-assisted Ag sintering can reach ≈ 200–300 $W{\cdot}m^{-1}{\cdot}K^{-1}$ depending on densification quality. Sintered Cu (including Ag-coated Cu) offers lower cost and ~150–200 $W{\cdot}m^{-1}{\cdot}K^{-1}$ though inadequate oxide management degrades TC and reliability (can surpass ~200 $W{\cdot}m^{-1}{\cdot}K^{-1}$ with stringent oxide control). Both Ag and Cu sinters show robust HTS/PCT/TST performance in SiC/GaN power packages the principal trade-off lies between the higher cost and potential electromigration risk of Ag and the oxidation control and process complexity associated with Cu systems [22–26,29,107].

4.2.2. Transient liquid phase sintering

Ag–Sn, Cu–Sn, or Ag–In couples transiently melt and interdiffuse to form intermetallic-rich joints whose final solidus temperature exceeds typical LED operating temperatures, producing thin, reflow-robust bond lines at lower clamp pressures than sintering. Because intermetallic compounds dominate the microstructure, the effective k⊥ is generally lower than that of dense sintered Ag. However, TLPS joints offer excellent thermal and mechanical stability and are particularly suitable where assembly pressure is limited or solder-like manufacturing workflows are required [27,28].

4.2.3. Indium foils and soft-metal interlayers

Bulk indium exhibits a room-temperature TC of approximately 86 $W{\cdot}m^{-1}{\cdot}K^{-}1$, enabling thin, highly conformal, and readily reworkable metal contacts suitable for TIM 1.5 interfaces (located between the package heat spreader and the substrate) as well as for TIM 2 applications. The R''_{TIM} is governed by surface condition and clamp pressure: clean mating surfaces are required, and R''_{TIM} decreases with increasing pressure; micro-embossed (patterned) foils concentrate load to promote localized plastic deformation, achieving a given R''_{TIM} at lower pressures and continuing to decrease as interfacial creep occurs under sustained load. For high-cycle, multi-insertion use (e.g., burn-in/test), device-side aluminium-clad indium foils are supplied to prevent adhesion/residue and enhance handling durability, with only the added barrier layer representing a minor thermal penalty. Extrusion is controlled primarily through materials/operating choices, selecting an alloy whose melting point comfortably exceeds the maximum service temperature and avoiding excessive pressure [165,166].

In summary, sintered Ag maximizes thermal performance and high-temperature stability; sintered Cu balances cost and TC with careful oxide control; TLPS suits pressure-limited, reflow-compatible assembly; indium foils serve niches demanding the thinnest, most conformal, and reworkable bond lines.

4.2.4. Liquid metals and hybrids

Room-temperature Liquid Metals (LMs) based on gallium, indium, bismuth, tin, and their alloys have been deployed as TIMs in LED packages, commonly as pads or thin films that remain liquid at operating temperature to conformally fill asperities and eliminate interfacial voids [167,168]. Owing to metal-like TC (typically 1–80 $W{\cdot}m^{-1}{\cdot}K^{-1}$, with Ga–In alloys such as EGaIn ≈ 25–30 $W{\cdot}m^{-1}{\cdot}K^{-1}$) and extreme wetting/compliance, LMs can achieve low BLT and minimise ITR even under modest assembly pressures [167,169,170]. In addition to their high TC, many LM TIMs (particularly gallium-based alloys) offer several advantages, including low vapor pressure, sub-cooling capability, biocompatibility, environmental friendliness, softness, safety, high chemical stability, and small volume expansion [167,170,171].

Despite these advantages, practical implementation requires careful mitigation of Ga–Cu (and Ga–Al) corrosion and IMC, native oxide "skin" effects, leakage and fluid migration, and electrical shorting risks; therefore, barrier layers or encapsulation strategies are typically required. These interfacial challenges are fundamentally governed by oxide-layer formation and wettability effects, which strongly influence thermal transport and long-term stability [172,173]. Nickel barrier layers on copper effectively suppress Ga-induced corrosion. Further barriers to adoption include high density and relative cost, toxicity (particularly for In- and Bi-containing alloys), and end-of-life management concerns [167,174–176]. Hybridization strategies address these limitations while enhancing performance. Particulate-modified LMs (e.g., Ag-doped Ga and Bi–In–Sn alloys with ceramic additives such as WO_3) raise bulk TC to ≳ 45 W $\cdot m^{-}1{\cdot}K^{-1}$, increase viscosity to curb leakage/migration, improve interfacial bonding to copper, and demonstrably reduce LED T_j [177–179].

LM matrices loaded with surface-metallized diamond further boost heat dissipation with minimal leakage and are well-suited to HP LED modules [180]. Embedding LMs within polymers yields electrically safer constructs (LM-embedded elastomers (LMEE) and LM microgels) forming soft, printable pads that maintain thin BLTs and $R''_{TIM} \lesssim$ 4–5 $mm^2{\cdot}K{\cdot}W^{-1}$ under moderate pressure, with promising cycling/strain tolerance [181]. However, electrically resistive LM–polymer composites typically exhibit limited effective conductivity (~5.3 $W{\cdot}m^{-1}{\cdot}K^{-1}$) [182].

Reliability data are encouraging: LM TIMs have withstood 3000 h at 130 °C followed by 1500 thermal cycles between −40 °C and 80 °C [183]. Beyond passive interfaces, LMs also enable compact active cooling of HP LEDs via low-power, nearly noiseless electromagnetic pumping [184].

4.2.5. Metal–diamond

Diamond's exceptionally high intrinsic TC (≈ 2200 $W{\cdot}m^{-1}{\cdot}K^{-}1$) and very low CTE make it an attractive reinforcement for metal–diamond composites, most notably Cu/diamond and Ag/diamond, used in high-end heat spreaders and TIM blocks. Achieving high effective TC in

these systems depends critically on interfacial engineering to enhance wetting and minimise ITR at the metal–diamond boundary. Carbide-forming interlayers and coatings (e.g., W, Ti, and their carbides such as TiC and WC), together with suitable matrix alloying, are widely applied. When combined with hot pressing, pressure infiltration, or liquid-phase sintering, these approaches routinely yield bulk conductivities above 500 $W{\cdot}m^{-1}{\cdot}K^{-1}$ at practical densities. Recent W-coated architectures report TC $\approx$ 640 $W{\cdot}m^{-1}{\cdot}K^{-1}$ at <50 vol% diamond, highlighting the effect of optimised interfacial design rather than diamond loading alone. Remaining challenges include raw material cost, coating and processing complexity, and the poor machinability of diamond composites, which together restrict large-scale adoption [108–110].

4.2.6. *Metallic nanowires and foams*

Metallic nanowires (Ag, Cu) and open-cell foams provide lightweight and conformal thermal scaffolds for heat management. Ag nanowire–polymer composites exhibit lower wire–matrix ITR compared with carbon-based fillers, enabling substantial TC enhancement even at low volume fractions. However, recent studies indicate non-monotonic TC–loading behaviour governed by intra-network R_C and junction resistance between adjacent nanowires, rather than filler loading alone.

Complementary approaches using Cu foams infiltrated with LMs or PCMs exploit capillarity and mechanical compliance to achieve effective TC $\geq$50 $W{\cdot}m^{-1}{\cdot}K^{-1}$, together with added vibration damping, attributes beneficial for TIM and thermal storage assemblies [44]. These findings highlight that interface quality, network continuity, and infiltration uniformity are crucial for translating the intrinsic metal conductivity of these scaffolds into device-level performance.

4.3. *Engineered composite TIMs*

Engineered composite TIMs rely on matrix-based systems in which heat transport is governed not merely by filler loading, but by the deliberate design of conductive networks, interfacial chemistry, and microstructural architecture. Unlike conventional polymer TIMs discussed in Section 4.1, performance gains in these systems arise primarily from engineered percolation pathways, alignment strategies, hierarchical structuring, and interfacial modification aimed at reducing ITR within thin BLTs [16,17,185–187]. Recent studies emphasize strategies such as filler orientation, hybridization, and hierarchical structuring, which not only improve thermal stability and mechanical integrity but can also reduce TR by more than 40 % compared to random dispersions [20,188–190]. Such architecture-driven approaches enable substantial reductions in TR while maintaining dielectric integrity and mechanical compliance required for HP LED packaging [191–193].

Polymer-based matrices including epoxies, silicones, and thermoplastics form the foundation of these composite systems. Their intrinsic TC is low ($\approx$ 0.2–0.25 $W{\cdot}m^{-1}{\cdot}K^{-}1$ for unfilled epoxies), and therefore conductive fillers are required to establish effective heat pathways. Epoxy remains widely adopted due to its chemical resistance, mechanical robustness, electrical insulation, and formulation flexibility [51,95,194].

Current performance improvements in polymer composites are increasingly governed by microstructural and interfacial engineering rather than filler loading alone. Filler shape, orientation, contact quality, and interfacial chemistry strongly influence ITR and percolation pathway formation [18,36,195]. Based on filler size, polymer TIMs can be classified as micro-, meso-, and nanocomposites [196]; among these, PNCs are the most extensively investigated because they combine high TC with electrical insulation, low density, and ease of processing, making them highly suitable for LED packaging applications [58].

Thermal transport in PNC TIMs is governed by four coupled factors: (*i*) *filler loading and percolation behaviour*, (*ii*) *ITR at polymer–filler and filler–filler contacts*, (*iii*) *filler geometry (size/shape, aspect ratio) and orientation*, and (*iv*) *dispersion quality and rheology that ultimately determines BLT and void formation*. Effective medium models that account for ITR, such as the Nan–Birringer–Clarke–Gleiter model, describe the sharp increase in TC near the percolation threshold and its saturation at high filler concentrations where ITR and voids dominate [195,197]. Since the TC of the polymer matrix is far below that of typical fillers (>500 $W{\cdot}m^{-1}{\cdot}K^{-}1$), TC increases with filler content (Fig. 13); however, excessive loading leads to high viscosity, agglomeration, and porosity, which reduce workability and reliability [102,198–200].

Reducing ITR through surface passivation, coupling agents, or phonon-bridge interlayers is often more effective than further increasing filler content, particularly for thin BLTs typical of LED packaging [201]. High-aspect-ratio fillers such as h-BN platelets, CNTs, or BNNTs reduce percolation thresholds and junction density, while multimodal particle size distributions enhance packing density and connectivity [202,203]. Hybrid or synergistic systems (Fig. 14), where smaller fillers bridge gaps between larger flakes, create additional parallel heat-transfer routes [204,205]. Filler orientation is equally critical; parallel alignment can produce up to a fivefold increase in TC compared with perpendicular arrangements. Orientation control can be achieved through tensile stretching, electrospinning, freeze casting, electric or magnetic fields, hot pressing, nozzle-shear 3D printing, or ultrasonic standing waves, exploiting filler anisotropy to establish ordered conductive networks [102,161–163]. Although additive manufacturing improves scalability, maintaining consistent filler alignment under industrial production rates remains a challenging [163,164].

Based on structural design and filler type, advanced PNC TIMs can be broadly classified into three principal groups: electrically insulating ceramic composite networks, architected carbon-based frameworks, and hybrid multiscale filler systems. Collectively, these categories illustrate that achieving high thermal performance in HP LED packages requires coordinated optimisation of filler selection, network architecture, and interfacial engineering under practical constraints of electrical

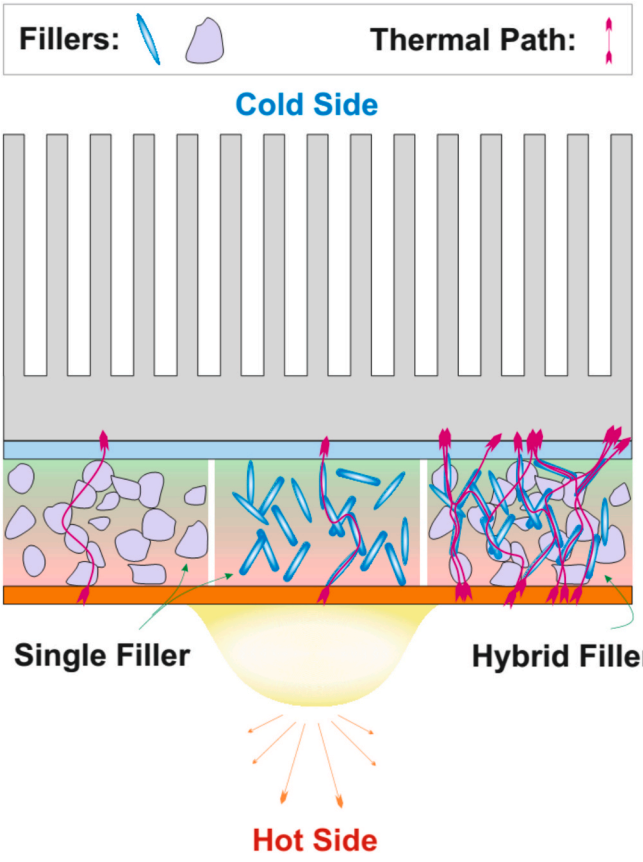

Fig. 13. Synergetic effect of fillers in a hybrid TIMs.

insulation, processability, and reliability.

4.3.1. Electrically insulating ceramic composite networks

When dielectric integrity is critical, ceramic-filled PNCs such as BN or AlN–epoxy composites are preferred because of their superior electrical insulation and stable TC [97,98]. Across polymer-based TIMs, thermal transport depends on constructing aligned and densified conduction networks while minimising interfacial losses within thin bond lines. For dielectric applications, oriented ceramic architectures are particularly effective. Uniaxially aligned h-BN/TPU laminates containing approximately 67 vol% BN achieve $k\perp \approx 43$ $W{\cdot}m^{-1}{\cdot}K^{-1}$, and compliant BN networks provide about 19 $W{\cdot}m^{-1}{\cdot}K^{-1}$ at $\leq$40 vol% [206,207].

AlN offers high intrinsic TC but is highly moisture-sensitive; hydrolysis to Al_2O_3 can reduce composite TC by roughly 5–6 times. This limitation is typically mitigated using hydrolysis-resistant passivation such as dense SiO_2 or polymer-derived ceramic coatings, which also enhance filler–polymer adhesion and long-term stability [198–201]. However, at high filler fractions, AlN composites often exhibit reduced electrical insulation that may persist even after silica coatings [93,200].

Common fillers employed in these systems include carbonaceous materials (graphite, graphene, diamond, CNTs), and ceramics (BN, SiC, AlN, Al_2O_3, BeO) [144,202,208,209]. For example, in Al_2O_3/epoxy systems, increasing filler size from 10 μm to 150 μm at 50 wt% improves TC by about 70 %, while increasing size from 10 μm to 44 μm at 75 wt% yields approximately 84 % improvement [159,160,210]. For electrically insulating TIM designs, aligned BN or passivated AlN fillers are preferred, using scalable alignment techniques such as shear or doctor-blade lamination for through-plane orientation, or magnetic-field alignment. Surface modification of AlN is essential to maintain hydrolysis resistance.

4.3.2. Architected carbon-based composite TIMs

Architected carbon frameworks provide highly conductive pathways but may compromise insulation in LED packages. In practice, aligned CNT networks, such as infiltrated vertically aligned CNT (VACNT) arrays, typically achieve $k\perp \geq 8$ W m^{-1} K^{-1} when dense architectures and strong interfacial bonding are obtained. VACNT arrays act as compliant, spring-like pillars that conformally bridge surface roughness; their array height, packing density, and tip/root bonding strongly influence both TR and cycling reliability [211–213].

Graphene-filled polymers generally exhibit TC values between 0.3 and 10 $W{\cdot}m^{-1}{\cdot}K^{-1}$, whereas oriented 3D graphene frameworks in epoxies can exceed 30 $W{\cdot}m^{-1}{\cdot}K^{-1}$ ($\approx$35–62 $W{\cdot}m^{-1}{\cdot}K^{-1}$). Vertically oriented graphene foams, graphene papers, and pyrolytic graphite sheets provide continuous through-plane heat pathways with $k\perp \approx$ 22–30 $W{\cdot}m^{-1}{\cdot}K^{-1}$ and exceptional in-plane spreading of $\approx$700–1000 $W{\cdot}m^{-1}{\cdot}K^{-1}$. Their high electrical conductivity requires dielectric isolation layers, for example, Al_2O_3 coatings, to prevent short-circuiting in LED packages [211–213].

Carbon fillers are attractive due to their low density and extremely high intrinsic TC (Single-Walled Carbon Nanotube (SWNT) $\geq$3000 $W{\cdot}m^{-1}{\cdot}K^{-1}$; Multi-Walled Carbon Nanotube (MWNT) $\approx$3000 $W{\cdot}m^{-1}{\cdot}K^{-1}$; graphene $\approx$3080–5150 $W{\cdot}m^{-1}{\cdot}K^{-1}$), enabling large conductivity enhancements even at low loadings, such as a 125 % TC increase at ~1 wt% SWNT in epoxy. Nevertheless, high ITR often restricts composite performance [93,214–217]. In high-flux applications, architected graphene or CNT frameworks are advantageous, provided that R_C is minimised through bonding and surface control, and electrical isolation is ensured using thin ALD-deposited Al_2O_3 or BN coatings [206,218–221].

Time-domain thermoreflectance measurements have been used to quantify and improve thermal boundary conductance at multilayer graphene–Si interfaces through interface modification, supporting graphene–Si integration in semiconductor and LED packages [222–226].

4.3.3. Hybrid and multiscale filler networks

Hybrid filler networks that combine multiple filler types, sizes, and morphologies can exploit synergistic effects to achieve both high TC and electrical insulation. By integrating 1D, 2D, or multimodal particle systems, these architectures densify conduction pathways, reduce percolation thresholds, and mitigate ITR while maintaining processability. In particular, boron nitride nanosheets (BNNSs), which are 2D plate-like structures with high intrinsic TC and excellent dielectric properties, can be combined with 1D BNNTs to form 1D–2D hybrid bridges that enhance thermal percolation. Such BNNT–BNNS composites, as well as AlN-sphere/BN-flake blends, achieve TC values of approximately 10 $W{\cdot}m^{-1}{\cdot}K^{-1}$ at processable filler loadings while maintaining electrical insulation [227]. In general, achieving ~10 $W{\cdot}m^{-1}{\cdot}K^{-1}$ in BNNT–PNCs requires either high overall BN loading or strongly aligned percolated architectures, which often increase viscosity and reduce mechanical compliance.

BNNTs combine low dielectric constant and excellent oxidation resistance, but high ITR and limited percolation often restrict TC in PNCs to ~1–4 $W{\cdot}m^{-1}{\cdot}K^{-1}$ at $\leq$30–40 wt% (e.g., epoxy-impregnated BNNT sheets reach ~2–3 $W{\cdot}m^{-1}{\cdot}K^{-1}$) [228–230]. Architected or hybrid networks can partially overcome these limitations. BNNT–BNNS/epoxy composites achieve ~2.6–3.4 W m^{-1} K^{-1} at 1 wt% BNNT + 30 wt% BNNS, and integrating BNNTs into functionalized BNNS frameworks yields $k\perp \approx 5.8$ $W{\cdot}m^{-1}{\cdot}K^{-1}$ at 40 wt% with in-plane TC ≈ 50 $W{\cdot}m^{-1}{\cdot}K^{-1}$ [227,231]. Exceptional co-networks such as BNNT–cellulose nanofiber papers can reach >20 $W{\cdot}m^{-1}{\cdot}K^{-1}$ at ~ 25 wt% BNNT [214].

Metallic fillers provide only modest TC gains and generally require 50–70 vol% to reach 1–5 $W{\cdot}m^{-1}{\cdot}K^{-1}$, while also facing oxidation and insulation limitations. Typical ranges include Al–epoxy 1–4 $W{\cdot}m^{-1}{\cdot}K^{-1}$ (up to 3–4 $W{\cdot}m^{-1}{\cdot}K^{-1}$ at high loadings) and Cu–epoxy 2–8 $W{\cdot}m^{-1}{\cdot}K^{-1}$; metal–graphene hybrids can reach 9–13 $W{\cdot}m^{-1}{\cdot}K^{-1}$ [39,98,232–237].

As R_C can dominate at low BLT, interfacial engineering through coupling agents, conformal coatings, and phonon-bridge structures can be more effective than adding extra filler, lowering R_C by about 70 % to $\approx$38 $mm^2{\cdot}K{\cdot}W^{-1}$ [201]. Regardless of composition, the overall thermal performance of a TIM is often constrained by R_C at the bonded interfaces, which is highly sensitive to surface roughness, wetting behaviour, and the level of applied clamping pressure.

Table 5 summarizes representative composite TIMs relevant to LED applications, grouped according to filler class. In general, hybrid filler systems demonstrates higher effective k⊥ than single-filler formulations due to improved network connectivity and reduced interfacial losses. For LED interfaces between metal-core printed circuit boards (MCPCBs) and heat sinks, as well as for encapsulation regions, dielectric ceramic-based systems (e.g., BN, AlN, Al_2O_3) are typically preferred because they combine high thermal conduction with electrical insulation. In contrast, metal- or carbon-based composites may achieve higher intrinsic conductivity but require dielectric barrier strategies in practical LED assemblies to avoid short-circuiting.

4.4. Architecture-driven and emerging TIM concepts

4.4.1. Nano-architected and contact-engineered interfaces

Beyond bulk TC, contact engineering through micro and nano architectures such as liquid-infused nanostructured composites (LINC), bridged or vertically aligned nanowire arrays, and graphene–nanowire "sandwich" joints has achieved record low ITR values. In LINC designs, double-sided vertically aligned Cu nanowire scaffolds infused with a tailored thermal liquid exhibit ITR < 1 $mm^2{\cdot}K{\cdot}W^{-1}$ under moderate contact pressures and maintain excellent thermal cycling durability between −55 °C and 125 °C [100].

Complementary bridged constructs, exemplified by 3D graphene–Cu nanowire sandwich joints, combine compliant low-stiffness nanowire contacts with highly conductive carbon layers, achieving TR of approximately 0.24 $mm^2{\cdot}K{\cdot}W^{-1}$ while enduring more than 1000 thermal cycles. These results highlight the potential of contact-engineered

Table 5
Representative composite TIMs for LED modules with reported k⊥ and electrical insulation characteristics.

Matrix	Filler(s)	Fraction†	k⊥ ($W \cdot m^{-1} \cdot K^{-1}$)	Electrical insulation	Ref.
▼ ***Metal filler TIMs (use only with an electrical barrier in LED modules)***					
Epoxy	Ag	77 wt% or 28 vol%	3.0	No	[238]
Epoxy	Al	50 vol%	Not reported — cured > uncured		[39]
Polyacrylate (UV–cured)	Cu nanowires (ultralong)	0.9 vol%	2.46	No	[239]
▼ ***Carbon filler TIMs (conductive—use only with a barrier)***					
Epoxy	Graphite	30 wt%	1.7	No	[240]
Epoxy	GNP	25 wt%	2.67	No	[241]
Silicone	GNs	1.5 wt%	2.7	No	[235]
▼ ***Ceramic filler TIMs (dielectric—preferred for LED TIMs)***					
Epoxy	Al_2O_3	50 wt%	0.35–0.65	Yes	[210]
HDPE	BN (platelets)	35 vol%	0.87	Yes	[242]
Epoxy	BN (modified)	60 wt%	1.052	Yes	[243]
Epoxy	AlN	40 vol%	1.3	Yes	[200]
Epoxy	Al_2O_3	75 wt%	2.06	Yes	[51]
Epoxy	BNNT	30 wt%	2.77	Yes	[93]
Epoxy	AlN	57 vol%	3.39	Yes	[244]
CNF	BNNT	40 wt%	4.71	Yes	[214]
▼ ***Hybrid filler TIMs (mostly dielectric; check composition)***					
HDPE	BN + Al_2O_3	35 vol%+7 vol%	1.02	Yes	[242]
PPS ‡	BN + MWCNT	50 wt%+1 wt%	1.74	No (CNTs)	[245]
Epoxy	BN + AlN	40 vol%	2.4	Yes	[246]
Epoxy	Al2O3 + BNNS	65 vol%	2.43	Yes	[53]
Epoxy	BN + Al_2O_3 + SiC	60 vol%	4.3	Likely Yes*	[247]
Epoxy	BN + Al_2O_3	5.32 vol%+ 68.82 vol%	4.4	Yes	[248]
PDMS	BNNS + RC	27.05 vol% BNNS	5.13	Yes	[249]

† wt is weight fraction, and vol. is volume fraction.
‡ PPS = polyphenylene sulfide; *RC = regenerated cellulose.*

architectures for reducing interface losses and improving the reliability of high-performance TIM assemblies [101].

4.4.2. MXene–enabled architectures

Among emerging two-dimensional materials, MXenes have recently attracted attention for TIM applications due to their unique structural and interfacial properties. 2D MXenes, particularly $Ti_3C_2T_x$, provide high-aspect-ratio flakes with surface terminations that promote dispersion, interfacial coupling and network formation in composite TIM systems. Although dense MXene films exhibit only modest room-temperature TC (approximately 3 $W \cdot m^{-1} \cdot K^{-1}$) on their own, architected aerogels, laminates, and hybrid structures incorporating BN, graphene, or polymer matrices can generate more effective heat transport pathways while retaining the thin, conformal; character desirable for interfacial applications. Recent work on $Ti_3C_2T_x$ MXenes/graphene hybrid films further shows the interfacial self-assembly can produce uniform and continuous ultra-thin heterostructures through a scabble route, highlighting the boarder potential of MXene-based hybrid sheets and interlayers for next-generation thermal-management architectures [250].

MXene frameworks may also serve as multifunctional hosts in composite thermal systems. In particular, MXene-containing aerogels and bio-mimetic composite structures have been explored not only for heat transport, but also for phase-change integration, mechanical compliance, and multifunctional behaviour. This broadens the role of MXenes from simple conductive fillers to architecture-defining components within advanced TIM concepts [251,252].

However, oxidation susceptibility and intrinsic electrical conductivity remain significant major limitations for LED-relevant TIM use. Recent studies emphasise that trapped water, reactive surface sites, and defect-rich structures can accelerate oxidation and degrade long-term performance. Accordingly, surface passivation, polymer encapsulation, defect-minimised synthesis, and electrically insulating hybridisation strategies remain essential, particularly for HP LEDs [253]. At the same time, emerging developments in additive manufacturing, interfacial engineering, and multifunctional MXene composites suggest that these materials may become increasingly important in adaptive, printable, and architecture-driven TIM systems [254,255].

4.4.3. Shape-stable and advanced phase-change TIM architectures

Advanced phase-change TIMs (PCTIMs) increasingly employ shape-stabilised architectures such as expanded graphite (EG), BN networks, MXene aerogels, and polymer microcapsules that suppress melt leakage while enabling pressure-activated wetting during softening, thereby reducing interfacial resistance and pump-out compared with neat waxes or oils. Designed for thin BLT and compatibility with common surface finishes, these composites offer improved lateral heat spreading and cycling stability, particularly when combined with EG/BN frameworks or microencapsulated PCMs [111].

A key design parameter is precise melt-point selection. When the phase-change temperature aligns with the device operating window (for example, in LEDs), PCTIMs provide effective transient thermal buffering during power cycling [112]. Form-stable PCM membranes that remain solid in the off state but melt under thermal stress conform to surface asperities, filling voids and enhancing k⊥ [113]. In HP modules, embedding PCMs within high-conductivity scaffolds such as copper foams mitigates surge-induced thermal excursions, lowering peak T_j by approximately 35 °C [256]. Overall, these developments emphasise shape stability, controllable wetting, and targeted melting temperature as complementary strategies for reliable, low-BLT PCTIMs with minimal leakage and durable performance.

4.4.4. Smart, adaptive, bio-inspired TIM concepts

Emerging bio-inspired TIMs utilise gecko-like dry adhesives and mussel-inspired surface chemistries to maximise real contact area at low clamping loads while maintaining removability. These interfaces can simultaneously damp vibration and reduce R_C. Smart TIMs integrate stimuli-responsive polymers activated by temperature, strain, or mag-

netic fields, functioning as thermal switches or self-healing matrices. LM-based elastomers are notable examples, offering adaptive thermal pathways and simplified maintenance strategies for next-generation thermal management systems [105].

Overall, emerging TIM technologies are increasingly focused on multifunctionality and interface engineering rather than solely maximising bulk thermal conductivity. Hybrid architectures combining high-conductivity fillers, compliant matrices, and adaptive interfaces are particularly promising for next-generation HP LED systems. In this context, materials such as liquid metals, MXene-based composites, and phase-change-enabled structures represent key directions for future development.

5. Conceptual design and fabrication roadmap for an LED-grade electrically insulating TIM

This section presents a conceptual design and manufacturing roadmap illustrating how an electrically insulating, high-k⊥ TIM could be realised for HP LED applications. The approach is not reported as an experimentally validated process within the present manuscript but serves to integrate the material, architectural, and reliability principles discussed in Sections 3 and 4.

The development target us an LED-grade dielectric TIM capable of achieving $k\perp \geq 10\ W{\cdot}m^{-1}{\cdot}K^{-1}$ at a BLT of approximately 50–150 μm, while maintaining electrical insulation and mechanical compliance. The stages outlined below describe a feasible pathway toward this performance window.

5.1. Performance target definition and 1D thermal stack analysis

To define an LED-relevant performance target for an electrically insulating TIM, a simplified 1D steady-state thermal resistance model is employed to quantify the T_j benefit of reducing R_{TIM}. This analytical estimate provides a first-order design benchmark linking k⊥, BLT, and RC to T_j control.

Consider a representative interface area $A = 1\ cm^2$ and steady heat dissipation $Q = 30$ W, typical of compact HP LED modules. A baseline polymer-based TIM layer with $k\perp = 3\ W{\cdot}m^{-1}{\cdot}K^{-1}$ and BLT = 150 μm yields a bulk thermal resistance, which corresponds to R_{bulk} of 0.5 $K{\cdot}W^{-1}$. If R_C of 10 $mm^2{\cdot}K{\cdot}W^{-1}$ are assumed at each interface, R_{TIM} becomes 0.7 $K{\cdot}W^{-1}$ (see Eq. (1)).

In contrast, an aligned BNNT/BNNS–epoxy concept achieving $k\perp = 10\ W{\cdot}m^{-1}{\cdot}K^{-1}$ at a reduced BLT of 75 μm results in a R_{bulk} of approximately 0.075 $K{\cdot}W^{-1}$. Assuming improved R_C of 5 $mm^2{\cdot}K{\cdot}W^{-1}$ at each interface due to enhanced conformity and surface wetting, R_{TIM} becomes 0.175 $K{\cdot}W^{-1}$.

The resulting T_j reduction is therefore: $\Delta T_j = Q{\cdot}\Delta R_{TIM} \approx 15.7$ °C.

Although this calculation is illustrative and R_{TIM} remains strongly dependent on clamping pressure, surface finish, and ageing conditions, the estimate clearly demonstrates that simultaneous reduction of BLT and R_C can yield substantially larger thermal benefits than increasing filler loading alone. The analysis therefore supports a practical design target of achieving $k\perp \geq 10\ W{\cdot}m^{-1}{\cdot}K^{-1}$ at BLT ≤100 μm with controlled R_C in electrically insulating LED TIMS.

5.2. Conceptual fabrication pathway

To realise the performance window defined in Section 5.1, a scalable fabrication route must integrate material formulation, microstructural alignment, interfacial engineering, and manufacturing compatibility. The following staged pathway illustrates how an electrically insulating, high-k⊥ TIM could be fabricated for HP LED applications while maintaining thin BLT and mechanical compliance.

5.2.1. Material formulation

A latent-cure epoxy matrix is selected to ensure extended pot life and controlled curing kinetics, and compatibility with automated dispensing or film casting processes. The filler system is designed to construct a continuous through-plane thermal network while preserving dielectric integrity and processability. The proposed hybrid architecture combines:

- 1D BNNTs to form the primary thermally conductive scaffold,
- 2D BNNSs to bridge inter-bundle gaps and enhance percolation, and
- Secondary ceramic fillers such as Al_2O_3 or AlN to improve packing density, dielectric strength, and dimensional stability.

To minimise ITR, silane coupling agents or polymer compatibilisers are incorporated to enhance filler–matrix adhesion and dispersion uniformity. Rheological tuning is critical to achieve sufficient shear-thinning behaviour for vacuum infiltration or direct-ink writing (DIW), depending on the intended manufacturing scale [257].

5.2.2. Scaffold formation via freeze-casting

A pH-controlled aqueous BNNT/BNNS slurry is first prepared to promote uniform dispersion and minimise agglomeration. Unidirectional or radially controlled freeze-casting, followed by freeze-drying, produces a porous, vertically aligned scaffold with 50–70 vol% open porosity [55].

This architecture establishes a continuous through-plane network that reduces phonon scattering and enhances k⊥. The freezing direction governs orientation and anisotropy, thereby allowing tuning of the balance between k⊥ and in-plane thermal spreading.

The resulting porous framework acts as a mechanically compliant, thermally continuous skeleton that is subsequently infiltrated with the polymer matrix.

5.2.3. Epoxy infiltration and curing

The aligned scaffold is vacuum infiltrated with the low-viscosity latent-cure epoxy to ensure complete pore filling and minimise void formation. A two-stage curing cycle is employed:

- An initial pre-cure at approximately 80 °C stabilise geometry, followed
- A post-cure at 130–150 °C under mild pressure to promote cross-linking and mechanical integrity.

The composite film is then cast or calendared to the desired BLT of 50–150 μm using release liners, enabling straightforward handling and integration into MCPCBs or heat spreader interfaces. Cross-sectional imaging using scanning electron microscopy or X-ray computed tomography should verify continuous vertical filler pathways and uniform matrix infiltration [258].

5.2.4. Additive manufacturing variant

As an alternative to freeze-casting, a shear-thinning DIW epoxy ink containing hybrid fillers at approximately 15–35 vol% may be directly printed into predefined pad geometries or mesoscale pillar structures.

Under assembly, these printed structures pressure to achieve the target BLT. While preserving vertical alignment of thermally conductive pathways. In situ dual-zone heating can initiate partial gelation during printing, followed by hot-press consolidation and final curing.

This approach enables pattern customisation, minimises material waste, and supports integration with automated LED assembly processes [259].

Fig. 14 summarises the sequential fabrication strategy integrating material formulation, scaffold alignment, matrix infiltration, and scalable processing routes for LED-compatible dielectric TIMs.

5.3. Degradation mapping and reliability-aware selection

Reliable operation of HP LED modules depends not only on the initial

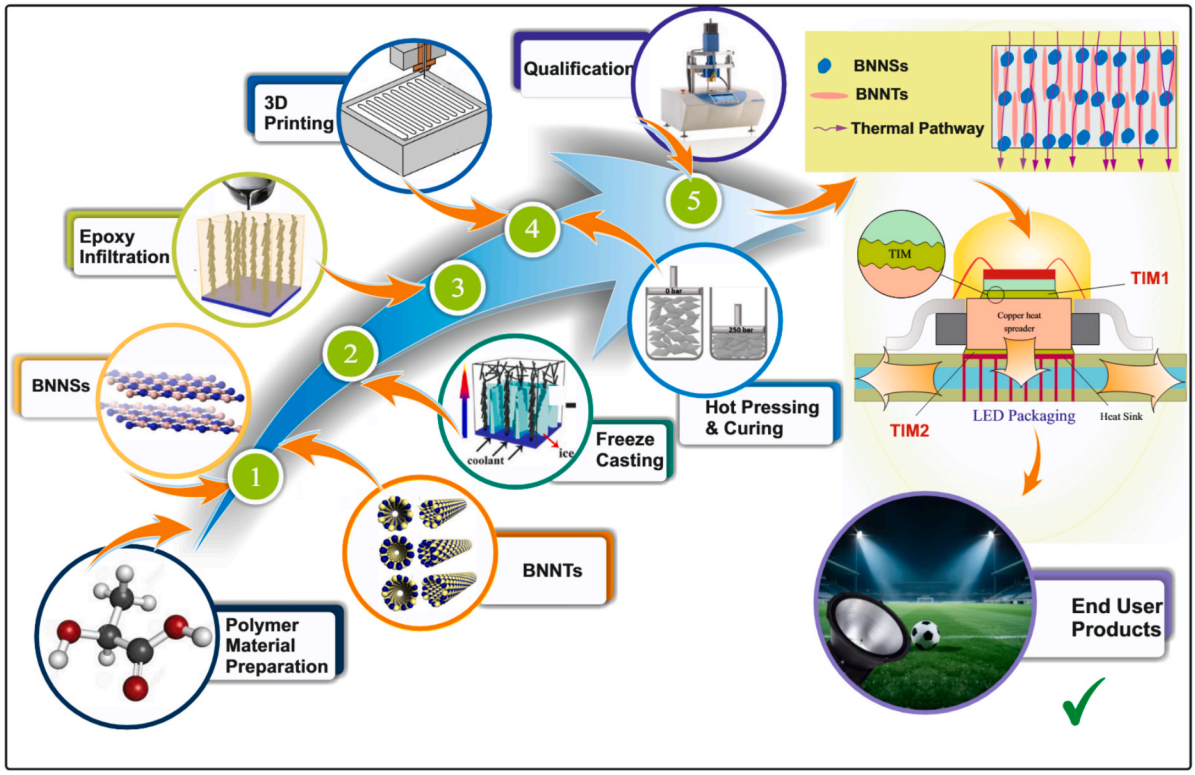

Fig. 14. Illustration of the sequential fabrication stages for an LED-grade, electrically insulating TIM, from material preparation to LED packaging and end-use applications.

thermal performance of the TIM but also on its long-term stability under thermal cycling, humidity exposure, and mechanical loading. Different TIM classes exhibit distinct degradation mechanisms that can progressively increase interfacial thermal resistance or lead to mechanical failure. To assist reliability-aware materials selection, Table 6 maps common degradation modes of TIMs to their primary thermal consequences and typical LED-level symptoms. This practical linkage between material degradation and device behaviour helps identify potential reliability risks during TIM selection and system design.

5.4. Qualification and reliability framework

Thermal performance should be quantified using ASTM D5470 steady-state methods to determine k⊥ and interface resistance as a function of clamping pressure. JESD51-14 testing under LED operating conditions further validates junction-to-case thermal resistance.

Reliability evaluation should include:

- Pump-out and dry-out tests for cured and uncured systems,
- Hydrolysis and corrosion screening for AlN/BN composites,
- Thermal cycling between −40 °C and 125 °C and high-temperature storage above 130 °C, and
- adhesion and mechanical compliance testing under repeated reflow or service cycles.

Compared with uncured greases or gels, cured BNNT/BNNS-epoxy systems are expected to demonstrate superior shape retention, lower R_{TIM}, and improved long-term stability, making them suitable candidates for HP reliability-critical LED modules [260,261].

Table 6
Practical mapping between common TIM degradation modes and LED-level symptoms or failure modes, intended to support reliability-aware materials selection.

TIM limitation/ degradation mode	Primary thermal consequence	Typical LED-level symptom/ failure mode
Pump-out/dry-out (greases, some gels)	R_{TIM} increases with time; localised hotspots	Accelerated lumen depreciation; colour shift; possible driver stress
Voiding/delamination (adhesives, solders, TLPS)	Localised TR and thermal-cycling stress	Intermittent flicker; sudden failure; package cracking
Leakage/exudation (PCMs)	Loss of contact area; contamination of optical surfaces	Optical contamination, reduced luminous efficacy; maintenance issues
Oxidation/corrosion (Cu, LM with Al)	Increase in interfacial R_C; interface embrittlement	Gradual rise in T_j; mechanical detachment over time
CTE mismatch/ fatigue (hard metallic joints)	Crack initiation and propagation; increase in R_{TIM}	Step-changes in TR; catastrophic open-circuit

5.5. Practical design guidelines for HP LED TIMs

Drawing on the material systems surveyed in Section 4 and the design principles outlined above, the following practical guidelines are proposed to support reliability-aware selection and optimisation of TIMs in HP LED modules.

Prioritise total R_{TIM} over bulk k⊥. A moderate k⊥ combined with thin BLT and low R_C often yields superior thermal performance compared with very high k⊥ at excessive bond-line thickness. Interface control and mechanical conformity are therefore as critical as intrinsic material conductivity.

Match electrical insulation requirements to interface function. TIM1 die-attach layers may employ metallic solutions in electrically isolated package architectures, whereas TIM2 interfaces commonly require dielectric fillers or insulating barriers to prevent current leakage between the LED substrate and the heat sink.

Treat reliability as a primary design constraint. Potential degradation mechanisms should be screened under representative power-cycling and

environmental conditions, including pump-out and dry-out in greases, leakage in PCMs, voiding and fatigue in soldered or TLPS joints, oxidation or corrosion in Cu- or Ga-based systems, and hydrolysis or creep in polymer composites.

Use LED-specific thermal metrics where available. Reporting junction-to-case thermal resistance, junction-to-sink resistance, clamping pressure, surface finish, and ageing history enables meaningful comparison between studies and supports translation to practical LED assemblies.

Co-design thermal and mechanical stacks. Surface flatness, clamping pressure, compliance layers, metallisation, and contact pressure distribution strongly influence R_C and long-term stability. Mechanical integration should therefore be considered concurrently with material selection.

6. Conclusion and outlook

TIMs are a critical determinant of thermal performance and reliability in HP LED packages, where interface-level heat transfer increasingly governs T_j and long-term device stability. This review has analysed the evolution of TIM technologies across four hierarchical families, including conventional conformable materials, bonded metallic interfaces, engineered composite systems, and emerging architecture-driven concepts.

Across these classes, the evidence consistently shows that LED-level performance is governed not only by intrinsic TC but by the coupled interaction of k⊥, BLT, and R_C. Consequently, optimisation of microstructure, interface wetting, and process control often yields greater reductions in R_{TIM} than increasing filler loading alone. Approaches that minimise BLT, promote filler alignment, and enhance real contact area have proven particularly effective in maintaining T_j within the desirable operating range of approximately 85–105 °C.

For electrically insulating LED interfaces, ceramic-based PNC systems incorporating BN or surface-passivated AlN fillers remain leading candidates due to their balanced thermal and dielectric performance. In contrast, bonded metallic TIMs such as sintered Ag, Cu, and TLPS joints provide ultra-low R_C for TIM1 or TIM2 interfaces when issues related to oxidation, wetting, and CTE mismatch stresses are carefully managed. Emerging concepts including nano-architected contacts, LM hybrids, and shape-stable PCTIM architectures further demonstrate the potential to reduce interfacial losses, mitigate thermal transients, and improve reliability under cyclic loading conditions.

Looking forward, several directions appear particularly promising for LED-grade TIM development:

i. *Hierarchical dielectric composites,* combining aligned BN networks with nanoscale bridges and toughened matrices to achieve high k⊥ while maintaining dielectric integrity at BLT $<$ 100 μm.
ii. *Data-driven formulation and optimization,* including physics-informed machine learning approaches to explore the coupled design space of k⊥–BLT–R_C–modulus–CTE and accelerate reliability screening.
iii. *Scalable architecture-controlled manufacturing*, such as freeze casting, vertical alignment, and DIW to enable ceramic or hybrid TIMs with k⊥ $\geq$ 10 $W{\cdot}m^{-1}{\cdot}K^{-}1$ at BLT values of approximately 50–150 μm.
iv. *Standardised reliability assessment*, using protocols such as ASTM D5470 and JESD51-14 combined with durability testing for pump-out, leakage, hydrolysis, corrosion, and −40 to 125 °C thermal cycling.
v. *Package-level co-design:* integrating TIM selection with semiconductor package architectures, particularly GaN and SiC systems, where surface finish, pressure distribution, and mechanical stack design strongly influence RC and long-term stability.

Overall, the future of TIMs for HP LED systems will depend on the integration of materials engineering, interface design, and scalable manufacturing strategies capable of delivering thin, reliable, and electrically safe interfaces. Such advances will enable lower T_j, improved efficiency, and longer service lifetimes in next-generation solid-state lighting systems.

CRediT authorship contribution statement

Armin Rahmati Darvazi: Writing – review & editing, Writing – original draft, Visualization, Resources, Investigation, Formal analysis, Data curation, Conceptualization. **Alireza Eslami Majd:** Writing – review & editing, Writing – original draft, Visualization, Resources, Methodology, Investigation, Data curation, Conceptualization. **Nduka Nnamdi Ekere:** Writing – review & editing, Supervision, Resources, Conceptualization. **Jin Wang:** Writing – review & editing, Visualization, Supervision, Resources, Funding acquisition.

Declaration of competing interest

The authors declare that they have no known competing financial interests or personal relationships that could have appeared to influence the work reported in this paper.

Data availability

Data will be made available on request.

References

[1] P. Ks, S. Basha, A. Chattopadhyay, K.K. Mahato, Recent advancements of light-emitting diodes in dairy industries, Trends Food Sci. Technol. 160 (2025) 105018, https://doi.org/10.1016/j.tifs.2025.105018.
[2] H. Chen, S.K. Yeboah, A. Dawodu, J.K. Dodoo, T. Zou, A systematic review of circular economy of artificial lighting and global sustainability, Energy Build. 347 (2025) 116314, https://doi.org/10.1016/j.enbuild.2025.116314.
[3] E. Pašić, N. Imamović, EFFICIENCY OF LED BULBS COMPARED TO CONVENTIONAL BULBS - ENERGY CONSUMPTION STUDY, 2024.
[4] Z. G, B. P, R.S. T, Update on the Status of LED-Lighting world market since 2018, (2021). https://doi.org/10.2760/759859 (online).
[5] Y. Zou, Y. Xia, H. Ren, C. Zhang, M. Wang, X. Tang, S. Ding, Heat dissipation design and optimization of high-power LED lamps, Therm. Sci. Eng. Prog. 37 (2023), https://doi.org/10.1016/j.tsep.2022.101587.
[6] S. Dang, H.H. Almahfoudh, A.M. Alajlan, H. Qasem, J. Wang, Y. Zhu, O.M. Bakr, B.S. Ooi, Q. Gan, Sky cooling for LED streetlights, Light Sci. Appl. 14 (2025) 100, https://doi.org/10.1038/s41377-024-01724-7.
[7] M. Hamidnia, Y. Luo, X.D. Wang, Application of micro/nano technology for thermal management of high power LED packaging – a review, Appl. Therm. Eng. 145 (2018), https://doi.org/10.1016/j.applthermaleng.2018.09.078.
[8] L. Xiang, Y. Cheng, X. Yu, Y. Fan, X. Yang, X. Zhang, B. Xie, X. Luo, High-performance thermal management system for high-power LEDs based on double-nozzle spray cooling, Appl. Therm. Eng. 231 (2023), https://doi.org/10.1016/j.applthermaleng.2023.121005.
[9] J. Zhang, J. Zhang, B. Xu, Q. Fu, C. Wang, H. Zhao, An improved LED junction temperature test method based on FCM, J. Phys. Conf. Ser. (2022), https://doi.org/10.1088/1742-6596/2395/1/012029.
[10] A. Chakraborty, R. Ganguly, M. Mitra, Non-Invasive Junction Temperature Measurement Using Forward Voltage Drop of High-Power pcLED Under Tropical Conditions, in: 2025 8th International Conference on Electronics, Materials Engineering & Nano-Technology (IEMENTech), 2025: pp. 1–6. https://doi.org/10.1109/IEMENTech65115.2025.10959524.
[11] G. Liu, Y. Zhang, C. Ma, Q. Tang, H. Li, S. Chen, J. Shen, Corrosion inhibition of Ga-based thermal interface materials with Ni coating on Cu substrate, Surf. Coat. Technol. 493 (2024) 131286, https://doi.org/10.1016/j.surfcoat.2024.131286.
[12] M. Liu, W. Li, W. Chen, M.S. Ibrahim, J. Xiong, G. Zhang, J. Fan, Junction temperature and luminous flux prediction for white LED array based on electrical-photo-thermal modeling, Case Stud. Therm. Eng. 54 (2024), https://doi.org/10.1016/j.csite.2023.103940.
[13] A. Rammohan, et al., Experimental analysis on estimating junction temperature and service life of high power LED array, Microelectron. Reliab. 120 (2021), https://doi.org/10.1016/j.microrel.2021.114121.
[14] Optraffic, Thermal stress testing LED lighting towers, (2025). https://optraffic.com/blog/thermal-stress-testing-led-lighting-towers/.
[15] J. Li, X. Zhang, C. Zhou, J. Zheng, D. Ge, W. Zhu, New applications of an automated system for high-power LEDs, IEEE/ASME Trans. Mechatron. 21 (2016), https://doi.org/10.1109/TMECH.2015.2487507.
[16] I.U. Rahman, S. Nardini, B. Buonomo, O. Manca, H. Khan, B. Siviero, Thermal interface materials: a promising solution for passive heat dissipation in electronic

appliances, Therm. Sci. Eng. Prog. 62 (2025) 103673, https://doi.org/10.1016/j.tsep.2025.103673.
[17] W. Xing, Y. Xu, C. Song, T. Deng, Recent advances in thermal interface materials for thermal management of high-power electronics, Nanomaterials 12 (2022) 3365.
[18] Y. Tu, B. Liu, G. Yao, H. Luo, X. Jia, J. Du, C. Xu, A review of advanced thermal interface materials with oriented structures for electronic devices, Electronics (Basel) 13 (2024), https://doi.org/10.3390/electronics13214287.
[19] Z. Li, J. Tan, J. Li, X. Ding, Y. Tang, A review on thermal management of light-emitting diodes: from package-level to system-level, Appl. Therm. Eng. 257 (2024) 124145, https://doi.org/10.1016/j.applthermaleng.2024.124145.
[20] W. Dai, Y. Wang, M. Li, L. Chen, Q. Yan, J. Yu, N. Jiang, C.-T. Lin, 2D materials-based thermal interface materials: structure, properties, and applications, Adv. Mater. 36 (2024) 2311335, https://doi.org/10.1002/adma.202311335.
[21] F. Sarvar, D. Whalley, P. Conway, Thermal Interface Materials - A Review of the State of the Art, in: 2006 1st Electronic Systemintegration Technology Conference, IEEE, 2006: pp. 1292–1302. https://doi.org/10.1109/ESTC.2006.280178.
[22] P. Panaccione, T. Wang, X. Chen, S. Luo, G.-Q. Lu, Improved heat dissipation and optical performance of high-power LED packaging with sintered nanosilver die-attach material, J. Microelectron. Electron. Packag. 7 (2010) 164–168.
[23] Heraeus Electronics, mAgic® DA295A: Low Temperature, Non-Pressure Dispensing Sinter Paste for Power Electronic Applications, (2025).
[24] Y. Zhao, B. Tolla, D. Katze, G. Castaneda, J. Wood, J.-A. Wilson, D. Brand, A hybrid pressure-less silver sintering technology for high-power density electronics, Imapsource Proc. 2022 (2023), https://doi.org/10.4071/001c.74591.
[25] K. Wakamoto, T. Namazu, Mechanical characterization of sintered silver materials for power device packaging: a review, Energies (Basel) 17 (2024), https://doi.org/10.3390/en17164105.
[26] T.F. Chen, K.S. Siow, Comparing the mechanical and thermal-electrical properties of sintered copper (Cu) and sintered silver (Ag) joints, J. Alloys Compd. 866 (2021) 158783, https://doi.org/10.1016/j.jallcom.2021.158783.
[27] Y. Wang, D. Xu, H. Yan, C.-F. Li, C. Chen, W. Li, Low-temperature copper sinter-joining technology for power electronics packaging: a review, J. Mater. Process. Technol. 332 (2024) 118526, https://doi.org/10.1016/j.jmatprotec.2024.118526.
[28] B. Zhang, Y. Xie, L. Wang, Y. Liu, Y. Wang, P. Niu, Y.-H. Mei, Pulsed electric current-assisted transient liquid phase sintering for extremely reliable Cu-Cu direct bonding, Mater. Sci. Eng. A 943 (2025) 148766, https://doi.org/10.1016/j.msea.2025.148766.
[29] S.K. Bhogaraju, A. Hanß, M. Schmid, G. Elger, F. Conti, Evaluation of silver and copper sintering of first level interconnects for high power LEDs, in: 2018 7th Electronic System-Integration Technology Conference (ESTC), 2018: pp. 1–8. https://doi.org/10.1109/ESTC.2018.8546499.
[30] L. Kim, M.W. Shin, Thermal analysis and design of high-power LED packages and systems, in: Sixth International Conference on Solid State Lighting, 2006. https://doi.org/10.1117/12.687681.
[31] K. Pashayi, H.R. Fard, F. Lai, S. Iruvanti, J. Plawsky, T. Borca-Tasciuc, High thermal conductivity epoxy-silver composites based on self-constructed nanostructured metallic networks, J. Appl. Phys. (2012), https://doi.org/10.1063/1.4716179.
[32] Y. Zhou, S. Wu, Y. Long, P. Zhu, F. Wu, F. Liu, V. Murugadoss, W. Winchester, A. Nautiyal, Z. Wang, Z. Guo, Recent advances in thermal interface materials, ES Mater. Manuf. (2020), https://doi.org/10.30919/esmm5f717.
[33] J. Hansson, T.M.J. Nilsson, L. Ye, J. Liu, Novel nanostructured thermal interface materials: a review, Int. Mater. Rev. 63 (2018), https://doi.org/10.1080/09506608.2017.1301014.
[34] N. Kaur, Thermal interface materials for efficient heat management in electronics, Appl. Therm. Eng. 287 (2026) 129415, https://doi.org/10.1016/j.applthermaleng.2025.129415.
[35] J.S. Lewis, T. Perrier, Z. Barani, F. Kargar, A.A. Balandin, Thermal interface materials with graphene fillers: review of the state of the art and outlook for future applications, Nanotechnology 32 (2021) 142003.
[36] B. Wei, W. Luo, J. Du, Y. Ding, Y. Guo, G. Zhu, Y. Zhu, B. Li, Thermal interface materials: from fundamental research to applications, SusMat 4 (2024) e239.
[37] X. Chen, L. Fan, X. Guo, H. Zheng, S. Cheng, P. Zheng, L. Zheng, X. Zhang, Y. Zhang, Self-adaptive thermal interface materials featuring low thermal resistance by combining phase change materials with magnetic field-induced filler alignment, Compos. B Eng. 304 (2025) 112687, https://doi.org/10.1016/j.compositesb.2025.112687.
[38] J. de D. Unión-Sánchez, M.J. Hermoso-Orzáez, M.J. Hervás-Pulido, B. Ogáyar-Fernández, Impact of thermal dissipation on the lighting performance and useful life of LED luminaires applied to urban lighting: a case study, Int. J. Environ. Res. Public Health 19 (2022), https://doi.org/10.3390/ijerph19020752.
[39] P. Anithambigai, S. Shanmugan, D. Mutharasu, T. Zahner, D. Lacey, Study on thermal performance of high power LED employing aluminum filled epoxy composite as thermal interface material, Microelectronics J. 45 (2014) 1726–1733, https://doi.org/10.1016/J.MEJO.2014.05.011.
[40] W. Han, M. Chen, W. Song, C. Ge, X. Zhang, Construction of hexagonal boron nitride@polystyrene nanocomposite with high thermal conductivity for thermal management application, Ceram. Int. 46 (2020) 7595–7601, https://doi.org/10.1016/j.ceramint.2019.11.259.
[41] D. Suh, S. Lee, C. Xu, A.A. Jan, S. Baik, Significantly enhanced phonon mean free path and thermal conductivity by percolation of silver nanoflowers, PCCP 21 (2019) 2453–2462, https://doi.org/10.1039/C8CP07229A.
[42] Y. Fu, J. Hansson, Y. Liu, S. Chen, A. Zehri, M.K. Samani, N. Wang, Y. Ni, Y. Zhang, Z. Bin Zhang, Q. Wang, M. Li, H. Lu, M. Sledzinska, C.M.S. Torres, S. Volz, A.A. Balandin, X. Xu, J. Liu, Graphene related materials for thermal management, 2D Mater. 7 (2020), https://doi.org/10.1088/2053-1583/ab48d9.
[43] H. Dai, R. Wang, Methods for measuring thermal conductivity of two-dimensional materials: a review, Nanomaterials 12 (2022), https://doi.org/10.3390/nano12040589.
[44] Y. Xue, X. Li, H. Wang, F. Zhao, D. Zhang, Y. Chen, Improvement in thermal conductivity of through-plane aligned boron nitride/silicone rubber composites, Mater. Des. 165 (2019) 107580, https://doi.org/10.1016/j.matdes.2018.107580.
[45] Y. Tang, D. Liu, H. Yang, P. Yang, Thermal effects on LED lamp with different thermal interface materials, IEEE Trans. Electron Devices 63 (2016) 4819–4824, https://doi.org/10.1109/TED.2016.2615882.
[46] C.J.M. Lasance, A. Poppe, others, Thermal management for LED applications, Springer, 2014.
[47] P. Liu, L. Li, L. Wang, T. Huang, Y. Yao, W. Xu, Effects of 2D boron nitride (BN) nanoplates filler on the thermal, electrical, mechanical and dielectric properties of high temperature vulcanized silicone rubber for composite insulators, J. Alloys Compd. 774 (2019), https://doi.org/10.1016/j.jallcom.2018.10.002.
[48] Q. Song, W. Zhu, Y. Deng, F. Hai, Y. Wang, Z. Guo, Enhanced through-plane thermal conductivity and high electrical insulation of flexible composite films with aligned boron nitride for thermal interface material, Compos. Part A Appl. Sci. Manuf. 127 (2019), https://doi.org/10.1016/j.compositesa.2019.105654.
[49] Z. Bo, C. Ying, H. Zhu, X. Wei, H. Yang, J. Yan, K. Cen, Bifunctional sandwich structure of vertically-oriented graphenes and boron nitride nanosheets for thermal management of LEDs and Li-ion battery, Appl. Therm. Eng. 150 (2019), https://doi.org/10.1016/j.applthermaleng.2019.01.068.
[50] X. He, Y. Wang, Highly thermally conductive polyimide composite films with excellent thermal and electrical insulating properties, Ind. Eng. Chem. Res. 59 (2020), https://doi.org/10.1021/acs.iecr.9b05939.
[51] P. Anithambigai, M.K. Dheepan Chakravarthii, D. Mutharasu, L.H. Huong, T. Zahner, D. Lacey, I. Kamarulazizi, Potential thermally conductive alumina filled epoxy composite for thermal management of high power LEDs, J. Mater. Sci. Mater. Electron. 28 (2017), https://doi.org/10.1007/s10854-016-5600-4.
[52] P. Anithambigai, D. Mutharasu, L.H. Huong, T. Zahner, D. Lacey, Synthesis and thermal analysis of aluminium nitride filled epoxy composites and its effective application as thermal interface material for LED applications, J. Mater. Sci. Mater. Electron. 25 (2014), https://doi.org/10.1007/s10854-014-2238-y.
[53] D. Zou, X. Huang, Y. Zhu, J. Chen, P. Jiang, Boron nitride nanosheets endow the traditional dielectric polymer composites with advanced thermal management capability, Compos. Sci. Technol. 177 (2019), https://doi.org/10.1016/j.compscitech.2019.04.027.
[54] C. Fu, Q. Li, J. Lu, S. Mateti, Q. Cai, X. Zeng, G. Du, R. Sun, Y. Chen, J. Xu, C. P. Wong, Improving thermal conductivity of polymer composites by reducing interfacial thermal resistance between boron nitride nanotubes, Compos. Sci. Technol. 165 (2018), https://doi.org/10.1016/j.compscitech.2018.07.010.
[55] T. Huang, Y. Li, M. Chen, L. Wu, Bi-directional high thermal conductive epoxy composites with radially aligned boron nitride nanosheets lamellae, Compos. Sci. Technol. 198 (2020) 108322, https://doi.org/10.1016/j.compscitech.2020.108322.
[56] T. Wang, G. Zhang, B. Zhang, S. Liu, D. Li, C. Liu, Oriented boron nitride nanosheet films for thermal management and electrical insulation in electrical and electronic equipment, ACS Appl. Nano Mater. 4 (2021), https://doi.org/10.1021/acsanm.1c00484.
[57] J. Chen, X. Huang, B. Sun, Y. Wang, Y. Zhu, P. Jiang, Vertically aligned and interconnected boron nitride nanosheets for advanced flexible nanocomposite thermal interface materials, ACS Appl. Mater. Interfaces 9 (2017) 30909–30917, https://doi.org/10.1021/acsami.7b08061.
[58] Z.G. Wang, W. Liu, Y.H. Liu, Y. Ren, Y.P. Li, L. Zhou, J.Z. Xu, J. Lei, Z.M. Li, Highly thermal conductive, anisotropically heat-transferred, mechanically flexible composite film by assembly of boron nitride nanosheets for thermal management, Compos. B Eng. 180 (2020), https://doi.org/10.1016/j.compositesb.2019.107569.
[59] D.L. Saums, Advances in thermal interface materials for power LED applications, in: A.P. Clemens, J.M. Lasance (Eds.), Thermal Management for LED Applications, 1st ed.,, Springer, New York, NY, 2013, pp. 299–346.
[60] P. Zhang, P. Yuan, X. Jiang, S. Zhai, J. Zeng, Y. Xian, H. Qin, D. Yang, A theoretical review on interfacial thermal transport at the nanoscale, Small 14 (2018) 1702769, https://doi.org/10.1002/smll.201702769.
[61] C.P. Feng, L.Y. Yang, J. Yang, L. Bai, R.Y. Bao, Z.Y. Liu, M.B. Yang, H.B. Lan, W. Yang, Recent advances in polymer-based thermal interface materials for thermal management: a mini-review, Compos. Commun. 22 (2020) 100528, https://doi.org/10.1016/J.COCO.2020.100528.
[62] V. Singhal, T. Siegmund, S.V. Garimella, Optimization of thermal interface materials for electronics cooling applications, IEEE Trans. Compon. Packag. Technol. 27 (2004) 244–252, https://doi.org/10.1109/TCAPT.2004.828587.
[63] Z. Dou, B. Zhang, P. Xu, Q. Fu, K. Wu, Dry-contact thermal interface material with the desired bond line thickness and ultralow applied thermal resistance, ACS Appl. Mater. Interfaces (2023), https://doi.org/10.1021/acsami.3c13298.
[64] X. Fan, Y. Sun, L. Huang, J. Xie, X. Zeng, C. Liu, L. Zhang, Y. Zhao, Improvement of interfacial thermal resistance between TIMs and copper for better thermal management, Surf. Interfaces 46 (2024) 103905, https://doi.org/10.1016/j.surfin.2024.103905.
[65] X. Jia, S. Wang, S. Li, C. Xu, J. Du, J. Zhou, Z. Cheng, F. Zhou, Y. Deng, B. Liu, X. Huai, Anti-leak, self-adaptive liquid metal-epoxy in-situ cured composites with

ultra-low thermal resistance via flexible droplet inclusions, Surf. Interfaces 42 (2023) 103335, https://doi.org/10.1016/j.surfin.2023.103335.
[66] J. Fan, Z. Ye, X. Zeng, J.-B. Xu, L. Ren, R. Sun, C.P. Wong, Predicting bond line thickness of polymeric thermal interface materials based on the rheological properties, J. Appl. Phys. 136 (2024), https://doi.org/10.1063/5.0209314.
[67] S. Jiong, J. Yun, J. Lee, J. Kim, Y. Choi, T. Kim, D. Lee, H. Eom, W. Choi, Nanosized boron nitride-incorporated polyvinyl alcohol composites with TEMPO-oxidized cellulose nanofibers as ultrathin thermal interface materials, Chem. Eng. J. 500 (2024) 157243, https://doi.org/10.1016/j.cej.2024.157243.
[68] K. Baran, A. Różowicz, H. Wachta, S. Różowicz, Modeling of selected lighting parameters of LED panel, Energies (Basel) 13 (2020) 3583, https://doi.org/10.3390/en13143583.
[69] M.G. Pecht, M.H. Chang, Failure mechanisms and reliability issues in LEDs, in: Solid State Lighting Reliability: Components to Systems, 2013. https://doi.org/10.1007/978-1-4614-3067-4_3.
[70] M. Sawant, A. Christou, Failure modes and effects criticality analysis and accelerated life testing of LEDs for medical applications, Solid State Electron. (2012), https://doi.org/10.1016/j.sse.2012.05.042.
[71] R. Wilcoxon, Does a 10°C Increase in Temperature Really Reduce the Life of Electronics by Half?, Electronics Cooling Magazine (2017). www.electronics-cooling.com/2017/08/10c-increase-temperature-really-reduce-life-electronics-half/.
[72] Andy Chen, How to Properly Evaluate Junction Temperature with Thermal Metrics, Application Report, Texas Instruments SLUA844B (2019).
[73] X.C. Tong, in: Advanced Materials for Thermal Management of Electronic Packaging, Springer Science & Business Media, 2011, https://doi.org/10.1007/978-1-4419-7759-5.
[74] TT Electronics | Optek Technology, Managing Junction Temperature of High-Power Visible Light Emitting Diodes (LEDs), 1645 Wallace Drive, Suite 130, Carrollton, TX, USA 75006, 2016. https://www.ttelectronics.com/TTElectronics/media/ProductFiles/Application-Note/App-Note-228-Thermal-Management-of-Visible-LEDs.pdf.
[75] E.Y. Gatapova, G. Sahu, S. Khandekar, R. Hu, Thermal management of high-power LED module with single-phase liquid jet array, Appl. Therm. Eng. 184 (2021), https://doi.org/10.1016/j.applthermaleng.2020.116270.
[76] J.L.F. Barbosa, D. Simon, W.P. Calixto, Design optimization of a high power LED matrix luminaire, Energies (Basel) 10 (2017), https://doi.org/10.3390/en10050639.
[77] A. Caria, R. Fraccaroli, G. Pierobon, T. Castellaro, A. Huang, J. Magnien, J. Rosc, G. Lipák, G. Hantos, J. Hegedüs, C. De Santi, M. Buffolo, N. Trivellin, E. Zanoni, A. Poppe, G. Meneghesso, M. Meneghini, Long-term (8000 h) reliability and failures of high-power LEDs for outdoor lighting stressed at high ambient temperatures, Microelectron. Reliab. 168 (2025) 115634, https://doi.org/10.1016/j.microrel.2025.115634.
[78] CreeLED, Thermal Management of XLamp® LEDs, 2023. https://downloads.cree-led.com/files/da/x/XLamp-Thermal-Management.pdf.
[79] OSRAM Opto Semiconductors GmbH, Reliability and Lifetime of LEDs, (2013). https://www.osram.com/Graphics/XPic6/00102625_0.pdf.
[80] X. Kang, Y. Wang, Q. Huang, Y. Cui, C. Wang, C. Wen, J. Fan, Phase-change immersion cooling high power light emitting diodes and heat transfer improvement, Microelectron. Reliab. 79 (2017) 257–264, https://doi.org/10.1016/j.microrel.2017.05.033.
[81] D. Iero, M. Merenda, R. Carotenuto, G. Pangallo, S. Rao, G. Brezeanu, F.G. Della Corte, A technique for improving the precision of the direct measurement of junction temperature in power light-emitting diodes, Sensors 21 (2021), https://doi.org/10.3390/s21093113.
[82] K.R. Shailesh, C.P. Kurian, S.G. Kini, Junction temperature measurement of a LED street light using forward voltage method, in: 2014 International Conference on Advances in Electronics, Computers and Communications, ICAECC 2014, 2015. https://doi.org/10.1109/ICAECC.2014.7002455.
[83] X. Zhao, H. Gong, L. Zhu, Z. Zheng, Y. Lu, LED junction temperature measurement: from steady state to transient state, Sensors 24 (2024), https://doi.org/10.3390/s24102974.
[84] R. Hu, Z. Mao, H. Zheng, Q. Chen, S. Liu, X. Luo, A compact thermal model to predict the junction temperature of high power light emitting diode package, Proc. – Electron. Components Technol. Conf. (2012), https://doi.org/10.1109/ECTC.2012.6249079.
[85] J. Liu, Y. Mou, Y. Huang, J. Zhao, Y. Peng, M. Chen, Effects of bonding materials on optical–thermal performances and high-temperature reliability of high-power LED, Micromachines (Basel) 13 (2022) 958, https://doi.org/10.3390/mi13060958.
[86] C.M. Kim, Y.T. Kang, Cooling performance enhancement of LED (Light Emitting Diode) using nano-pastes for energy conversion application, Energy 76 (2014), https://doi.org/10.1016/j.energy.2014.08.039.
[87] Y. Zhang, E. Long, M. Zhang, A new thermal interface material: graphene–epoxy composite used for LED heat dissipation, Chiang Mai J. Sci. 45 (2018) 2459–2470.
[88] T. Ramesh, A.S. Praveen, P.B. Pillai, S. Salunkhe, Phase change material aided thermal scheming of high power LED: effect of PCM with varying pitch of hexagonal fins, Mater. Res. Innov. 26 (2022), https://doi.org/10.1080/14328917.2021.1984665.
[89] G. Liang, J. Zhang, S. An, J. Tang, S. Ju, S. Bai, D. Jiang, Phase change material filled hybrid 2D/3D graphene structure with ultra-high thermal effusivity for effective thermal management, Carbon N. Y. 176 (2021), https://doi.org/10.1016/j.carbon.2020.12.046.
[90] J. Koo, J. Hyeong, S. Kim, M. Rim, C. Sung, S. Seo, S.-E. Kim, S. Kim, D.-Y. Kim, K.-U. Jeong, Thermally conductive and self-healable phase change nanocomposites from phenylnaphthalene Monomer, and programmed heat transfer materials derived therefrom for advanced thermal management systems, Chem. Eng. J. 510 (2025) 161680, https://doi.org/10.1016/j.cej.2025.161680.
[91] J.K.S.M.D. Timmerman, The development and characterization of hybrid thermal/emi solutions for electronicsS, in: Proceedings of SMTA International, 2016: pp. 124–131.
[92] J. Gandhi, A.V. Pathak, Performance evaluation of thermal interface material for space applications, Appl. Mech. Mater. 110–116 (2011) 135–141, https://doi.org/10.4028/www.scientific.net/AMM.110-116.135.
[93] X. Huang, C. Zhi, P. Jiang, D. Golberg, Y. Bando, T. Tanaka, Polyhedral oligosilsesquioxane-modified boron nitride nanotube based epoxy nanocomposites: an ideal dielectric material with high thermal conductivity, Adv. Funct. Mater. 23 (2013), https://doi.org/10.1002/adfm.201201824.
[94] J. Due, A.J. Robinson, Reliability of thermal interface materials: a review, Appl. Therm. Eng. (2013), https://doi.org/10.1016/j.applthermaleng.2012.06.013.
[95] K.M. Razeeb, E. Dalton, G.L.W. Cross, A.J. Robinson, Present and future thermal interface materials for electronic devices, Int. Mater. Rev. 63 (2018) 1–21, https://doi.org/10.1080/09506608.2017.1296605.
[96] H.H. Wu, K.H. Lin, S.T. Lin, A study on the heat dissipation of high power multi-chip COB LEDs, Microelectronics J. 43 (2012), https://doi.org/10.1016/j.mejo.2012.01.007.
[97] J.M. Hutchinson, F. Román, A. Folch, Epoxy-thiol systems filled with boron nitride for high thermal conductivity applications, Polymers (Basel) 10 (2018), https://doi.org/10.3390/polym10030340.
[98] H. Chen, V.V. Ginzburg, J. Yang, Y. Yang, W. Liu, Y. Huang, L. Du, B. Chen, Thermal conductivity of polymer-based composites: fundamentals and applications, Prog. Polym. Sci. 59 (2016) 41–85, https://doi.org/10.1016/j.progpolymsci.2016.03.001.
[99] M.Z. Akhtar, M. Schmid, A. Zippelius, G. Elger, LEDs Lifetime Prediction Modeling: Thermomechanical Simulation for SAC305 and SAC105, in: 2024 25th International Conference on Thermal, Mechanical and Multi-Physics Simulation and Experiments in Microelectronics and Microsystems (EuroSimE), 2024: pp. 1–10. https://doi.org/10.1109/EuroSimE60745.2024.10491530.
[100] R. Cheng, Q. Wang, Z. Wang, L. Jing, A.V. Garcia-Caraveo, Z. Li, Y. Zhong, X. Liu, X. Luo, T. Huang, H.S. Yun, H. Salihoglu, L. Russell, N. Kazem, T. Chen, S. Shen, Liquid-infused nanostructured composite as a high-performance thermal interface material for effective cooling, Nat. Commun. 16 (2025) 794, https://doi.org/10.1038/s41467-025-56163-8.
[101] L. Jing, R. Cheng, R. Garg, W. Gong, I. Lee, A. Schmit, T. Cohen-Karni, X. Zhang, S. Shen, 3D graphene-nanowire "sandwich" thermal interface with ultralow resistance and stiffness, ACS Nano 17 (2023) 2602–2610, https://doi.org/10.1021/acsnano.2c10525.
[102] G.D. Goh, Y.L. Yap, S. Agarwala, W.Y. Yeong, Recent progress in additive manufacturing of fiber reinforced polymer composite, Adv. Mater. Technol. 4 (2019), https://doi.org/10.1002/admt.201800271.
[103] C. Wei, Q. Zhang, Z. Wang, W. Yang, H. Lu, Z. Huang, W. Yang, J. Zhu, Recent advances in MXene-based aerogels: fabrication, performance and application, Adv. Funct. Mater. 33 (2023), https://doi.org/10.1002/adfm.202211889.
[104] M. Wang, Y. Liu, H. Zhang, Y. Wu, L. Pan, Thermal conductivities of Ti3C2Tx MXenes and their interfacial thermal performance in MXene/epoxy composites – a molecular dynamics simulation, Int. J. Heat Mass Transf. 194 (2022) 123027, https://doi.org/10.1016/j.ijheatmasstransfer.2022.123027.
[105] J. Fan, S. Ding, X. Zeng, S. Gao, Z. Wen, X. Zeng, R. Sun, L. Ren, Gecko-inspired adhesive structures enable efficiently thermal conductance and vibration dissipation in a highly mismatched system, Chem. Eng. J. 445 (2022) 136754, https://doi.org/10.1016/j.cej.2022.136754.
[106] L. Chen, X. Shi, N. Yu, X. Zhang, X. Du, J. Lin, Measurement and analysis of thermal conductivity of $Ti_3C_2T_x$ MXene films, Materials 11 (2018), https://doi.org/10.3390/ma11091701.
[107] H.A. Martin, S. Libon, E.C.P. Smits, R.H. Poelma, W.D. van Driel, G. Zhang, Thermal characterization methodology for thin bond-line interfaces with high conductive materials, Therm. Sci. Eng. Prog. 53 (2024) 102754, https://doi.org/10.1016/j.tsep.2024.102754.
[108] S.Q. Jia, F. Yang, High thermal conductive copper/diamond composites: state of the art, J. Mater. Sci. 56 (2021) 2241–2274, https://doi.org/10.1007/s10853-020-05443-3.
[109] H.J. Cho, Y.-J. Kim, U. Erb, Thermal conductivity of copper-diamond composite materials produced by electrodeposition and the effect of TiC coatings on diamond particles, Compos. B Eng. 155 (2018) 197–203, https://doi.org/10.1016/j.compositesb.2018.08.014.
[110] Z. Abdallah, J.W. Pomeroy, E. Neubauer, M. Kuball, Thermal characterization of metal-diamond composite heat spreaders using low-frequency-domain thermoreflectance, ACS Appl. Electron. Mater. 5 (2023) 5017–5024, https://doi.org/10.1021/acsaelm.3c00771.
[111] D. Huang, G. Ma, Z. Yu, P. Lv, Q. Zhou, Q. Liu, C. Peng, F. Xiong, Y. Huang, Highly thermal conductive shape-stabilized composite phase change materials based on boron nitride and expanded graphite for solar thermal applications, RSC Adv. 13 (2023) 13252–13262, https://doi.org/10.1039/D3RA01166F.
[112] H. Huang, C. Wang, T. Wu, Z. Wu, J. Zheng, Phase change thermal interface materials with interface adaptability and self-healing properties, Surf. Interfaces 55 (2024) 105406, https://doi.org/10.1016/j.surfin.2024.105406.
[113] L. Zhang, X. Zhang, W. Hua, L. Gao, W. Xie, W. Zhang, A novel thermal interface membrane structure based on phase change material for thermal management of electronics, J. Energy Storage 61 (2023) 106819, https://doi.org/10.1016/j.est.2023.106819.

[114] W. Lee, J. Kim, A comprehensive review of research on organic-based phase-change thermal interface materials for thermal management of electric devices: methods, performance, and applications, Polym. Test. 142 (2025) 108677, https://doi.org/10.1016/J.POLYMERTESTING.2024.108677.
[115] R. Tao, P. Centellas, S. Romberg, A. Kotula, G. Holmes, A. Forster, C. Soles, R. Allen, E. Cetegen, W. Chen, others, Material Needs and Measurement Challenges for Advanced Semiconductor Packaging: Understanding the Soft Side of Science, IEEE Trans. Compon. Packaging Manuf. Technol. (2025).
[116] Y.-M. Ju, T.-W. Kim, S.-H. Lee, H.-J. Lee, J. Ahn, H.-S. Kim, Advanced WBG power semiconductor packaging: nanomaterials and nanotechnologies for high-performance die attach paste, Nano Converg. 12 (2025) 38, https://doi.org/10.1186/s40580-025-00503-3.
[117] L.A. Yeboah, P.A. Oppong, A. Abdul Malik, P.S. Acheampong, J.A. Morgan, R.A. A. Addo, B. Williams Henyo, Sustainable manufacturing and applications of wide-bandgap semiconductors—a review, Intell. Sustain. Manuf. 2 (2025) 10010.
[118] M.C.K. Swamy, Satyanarayan, A review of the performance and characterization of conventional and promising thermal interface materials for electronic package applications, J. Electron. Mater. 48 (2019), https://doi.org/10.1007/s11664-019-07623-7.
[119] I.P. Bakk, G. Borsoi, P.A. Favarolo, Thermal management of LED systems, E & i Elektrotechnik Und Informationstechnik (2013), https://doi.org/10.1007/s00502-012-0103-3.
[120] Y. Deng, J. Li, T. Qian, W. Guan, Y. Li, X. Yin, Thermal conductivity enhancement of polyethylene glycol/expanded vermiculite shape-stabilized composite phase change materials with silver nanowire for thermal energy storage, Chem. Eng. J. 295 (2016), https://doi.org/10.1016/j.cej.2016.03.068.
[121] Indium Corporation, Thermal Interface Materials, 2022. https://buy.solder.com/wp-content/uploads/2022/04/thermal_interface_materials_98104_r0.pdf.
[122] M. Schmid, A. Zippelius, A. Hanß, S. Böckhorst, G. Elger, Investigations on high-power LEDs and solder interconnects in automotive application: part II—reliability, IEEE Trans. Device Mater. Reliab. 23 (2023) 419–429, https://doi.org/10.1109/TDMR.2023.3300355.
[123] L. Li, X. Du, J. Chen, Y. Wu, Thermal fatigue failure of micro-solder joints in electronic packaging devices: a review, Materials 17 (2024), https://doi.org/10.3390/ma17102365.
[124] N.A.M.N. Aman, M.Z. Abdullah, L.W. Keat, O.C. Keang, Influence of die and lid shapes on void formation in solder thermal interface materials, Microelectron. Reliab. 173 (2025) 115847, https://doi.org/10.1016/j.microrel.2025.115847.
[125] X. Cheng, C. Liu, V.V. Silberschmidt, Numerical analysis of thermo-mechanical behavior of indium micro-joint at cryogenic temperatures, Comput. Mater. Sci 52 (2012) 274–281, https://doi.org/10.1016/j.commatsci.2010.12.026.
[126] A. Bar-Cohen, K. Matin, S. Narumanchi, Nanothermal interface materials: technology review and recent results, J. Electron. Packag. 137 (2015), https://doi.org/10.1115/1.4031602.
[127] M. Chen, T. Xu, S. Liu, C.P. Wong, Study on thermal conductive adhesives for high-power LEDs packaging, Proc. – Int. Sympos. Adv. Packaging Mater. (2011), https://doi.org/10.1109/ISAPM.2011.6105681.
[128] A. Eslami Majd, N.N. Ekere, A. Rahmati Darvazi, A. Amini Sedehi, Creep-fatigue lifetime estimation of efficient photovoltaic module ribbon interconnections, Microelectron. Reliab. 139 (2022) 114831, https://doi.org/10.1016/j.microrel.2022.114831.
[129] Z. Ma, D. Diwu, K. Wang, J. Mu, X. An, H. Wang, G. Guo, Y. Hu, J. Ren, L. Fan, Reliability analysis of solder joints in aerospace electronics: failure mechanism, modeling and evaluation, J. Fail. Anal. Prev. (2025), https://doi.org/10.1007/s11668-025-02271-y.
[130] C.N. Hsu, K.W. Lee, C.C. Chen, Using graphene-based grease as a heat conduction material for hectowatt-level leds: a natural convection experiment, Processes 9 (2021), https://doi.org/10.3390/pr9050847.
[131] H. Kang, H. Kim, J. An, S. Choi, J. Yang, H. Jeong, S. Huh, Thermal conductivity characterization of thermal grease containing copper nanopowder, Materials 13 (2020), https://doi.org/10.3390/MA13081893.
[132] S. Narumanchi, M. Mihalic, K. Kelly, G. Eesley, Thermal interface materials for power electronics applications, in: 2008 11th IEEE Intersociety Conference on Thermal and Thermomechanical Phenomena in Electronic Systems, I-THERM, 2008. https://doi.org/10.1109/ITHERM.2008.4544297.
[133] Y. He, J.A. Wang, C.L. Pei, J.Z. Song, D. Zhu, J. Chen, Novel epoxy-silicone thermolytic transparent packaging adhesives chemical modified by ZnO nanowires for HB LEDs, J. Nanopart. Res. 12 (2010), https://doi.org/10.1007/s11051-010-9895-4.
[134] A.A. Ivanov, A.Y. Khomaykov, K.N. Afonin, A.S. Chermoshentseva, Filled polyaluminosilicates application as dielectric layers in car headlight module design to provide required temperature conditions, J. Phys. Conf. Ser. (2020), https://doi.org/10.1088/1742-6596/1488/1/012019.
[135] T. Cui, Q. Li, Y. Xuan, P. Zhang, Preparation and thermal properties of the graphene-polyolefin adhesive composites: application in thermal interface materials, Microelectron. Reliab. (2015), https://doi.org/10.1016/j.microrel.2015.07.036.
[136] D. Lu, C. Liu, X. Lang, B. Wang, Z. Li, W.M.P. Lee, S.W.R. Lee, Enhancement of thermal conductivity of die attach adhesives (DAAs) using nanomaterials for high brightness light-emitting diode (HBLED), Proc. – Electron. Components Technol. Conf. (2011), https://doi.org/10.1109/ECTC.2011.5898585.
[137] J.P. You, Y. He, F.G. Shi, Thermal management of high power LEDs: Impact of die attach materials, in: Proceedings of Technical Papers - 2007 International Microsystems, Packaging, Assembly and Circuits Technology Conference, IMPACT, 2007. https://doi.org/10.1109/IMPACT.2007.4433607.
[138] K. Zhang, G.D. Xiao, Z. Zeng, C. Wan, J. Li, S. Xin, X. He, S. Deng, Y. Zhang, C. Cui, Y. He, L. Liu, C.S. Ku, M.M.F. Yuen, A novel thermally conductive transparent die attach adhesive for high performance LEDs, Mater. Lett. 235 (2019), https://doi.org/10.1016/j.matlet.2018.09.170.
[139] G. Bischak, C. Vogdes, Thermal management design criteria and solutions, in: Northcon/98. Conference Proceedings (Cat. No.98CH36264), 1998: pp. 128–133. https://doi.org/10.1109/NORTHC.1998.731524.
[140] R. Viswanath, V. Wakharkar, A. Watwe, V. Lebonheur, Thermal performance challenges from silicon to systems, Int. Technol. J. (2000).
[141] D. Blazej, Thermal interface materials, Electron. Cooling 9 (2003) 14–21.
[142] X.C. Tong, Thermal interface materials in electronic packaging, Springer Ser. Adv. Microelectron. (2011), https://doi.org/10.1007/978-1-4419-7759-5_8.
[143] J. Appert, Thermal Interface Materials Choosing Between Gels and Gap Filler Pads, Parker Hannifi Corporation, 2020.
[144] M. Li, L. Li, X. Hou, Y. Qin, G. Song, X. Wei, X. Kong, Z. Zhang, H. Do, J.C. Greer, F. Han, T. Cai, W. Dai, C. Te Lin, N. Jiang, J. Yu, Synergistic effect of carbon fiber and graphite on reducing thermal resistance of thermal interface materials, Compos. Sci. Technol. 212 (2021), https://doi.org/10.1016/j.compscitech.2021.108883.
[145] K. Górecki, P. Ptak, T. Torzewicz, M. Janicki, Influence of a thermal pad on selected parameters of power LEDs, Energies (Basel) 13 (2020), https://doi.org/10.3390/en13143732.
[146] M. Janicki, P. Ptak, T. Torzewicz, K. Górecki, Compact thermal modeling of modules containing multiple power LEDs, Energies (Basel) 13 (2020), https://doi.org/10.3390/en13123130.
[147] G. Mittal, S.J. Park, K.Y. Rhee, Acrylic pressure-sensitive adhesive reinforced with aluminum nitride and its thermal properties: effect of surface treatment and particle size, Coatings 10 (2020), https://doi.org/10.3390/coatings10020188.
[148] S. Chambers, What is the carrier or backing material on adhesive products?, 2020.
[149] IEEE GlobalSpec, Thermal interface materials for next-generation electronics, Pleasanton, 2021.
[150] D.D.L. Chung, Thermal interface materials, J. Mater. Eng. Perform. 10 (2001) 56–59, https://doi.org/10.1361/105994901770345358.
[151] K.C. Otiaba, N.N. Ekere, R.S. Bhatti, S. Mallik, M.O. Alam, E.H. Amalu, Thermal interface materials for automotive electronic control unit: trends, technology and R&D challenges, Microelectron. Reliab. 51 (2011), https://doi.org/10.1016/j.microrel.2011.05.001.
[152] X. Zhang, Z. Huang, B. Ma, R. Wen, M. Zhang, Y. Huang, M. Fang, Y.G. Liu, X. Wu, Polyethylene glycol/Cu/SiO_2 form stable composite phase change materials: preparation, characterization, and thermal conductivity enhancement, RSC Adv. 6 (2016), https://doi.org/10.1039/c6ra12890d.
[153] A.R.M. Siddique, S. Mahmud, B. Van Heyst, A comprehensive review on a passive (phase change materials) and an active (thermoelectric cooler) battery thermal management system and their limitations, J. Power Sources 401 (2018), https://doi.org/10.1016/j.jpowsour.2018.08.094.
[154] L. Fan, J.M. Khodadadi, Thermal conductivity enhancement of phase change materials for thermal energy storage: a review, Renew. Sustain. Energy Rev. 15 (2011), https://doi.org/10.1016/j.rser.2010.08.007.
[155] J.P. Gwinn, R.L. Webb, Performance and testing of thermal interface materials, Microelectronics J. 34 (2003) 215–222, https://doi.org/10.1016/S0026-2692(02)00191-X.
[156] Y. Tang, L. Lin, S. Zhang, J. Zeng, K. Tang, G. Chen, W. Yuan, Thermal management of high-power LEDs based on integrated heat sink with vapor chamber, Energy Convers. Manage. 151 (2017), https://doi.org/10.1016/j.enconman.2017.08.087.
[157] Y. Zhao, J. Liu, A. Wei, J. Li, High-power light-emitting diodes package with phase change material, IEEE Trans. Compon. Packaging Manuf. Technol. 4 (2014) 1747–1753, https://doi.org/10.1109/TCPMT.2014.2359621.
[158] S. Wu, T. Yan, Z. Kuai, W. Pan, Thermal conductivity enhancement on phase change materials for thermal energy storage: a review, Energy Storage Mater. 25 (2020), https://doi.org/10.1016/j.ensm.2019.10.010.
[159] A. Permal, M. Devarajan, H.L. Hung, T. Zahner, D. Lacey, K. Ibrahim, Controlled high filler loading of functionalized Al_2O_3-filled epoxy composites for LED thermal management, J. Mater. Eng. Perform. 27 (2018), https://doi.org/10.1007/s11665-018-3151-y.
[160] J. Felba, Thermally conductive nanocomposites, in: Nano-Bio- Electronic, Photonic and MEMS Packaging, 2020. https://doi.org/10.1007/978-3-030-49991-4_7.
[161] C. Huang, X. Qian, R. Yang, Thermal conductivity of polymers and polymer nanocomposites, Mater. Sci. Eng.: R: Rep. 132 (2018) 1–22, https://doi.org/10.1016/j.mser.2018.06.002.
[162] P. Kumar, S. Yu, F. Shahzad, S.M. Hong, Y.H. Kim, C.M. Koo, Ultrahigh electrically and thermally conductive self-aligned graphene/polymer composites using large-area reduced graphene oxides, Carbon N. Y. 101 (2016), https://doi.org/10.1016/j.carbon.2016.01.088.
[163] J. Chen, X. Gao, Directional dependence of electrical and thermal properties in graphene-nanoplatelet-based composite materials, Results Phys. 15 (2019), https://doi.org/10.1016/j.rinp.2019.102608.
[164] J. Ji, S.W. Chiang, M. Liu, X. Liang, J. Li, L. Gan, Y. He, B. Li, F. Kang, H. Du, Enhanced thermal conductivity of alumina and carbon fibre filled composites by 3-D printing, Thermochim Acta 690 (2020), https://doi.org/10.1016/j.tca.2020.178649.
[165] A. MacKie, Indium corporation: igniting an electronics materials renaissance in upstate New York, IEEE Power Electron. Mag. 7 (2020), https://doi.org/10.1109/MPEL.2020.2985855.

[166] I. Corporation, Heat-Spring® | Compressible Thermal Interface Materials (TIMs), (2025). https://www.indium.com/products/thermal-interface-materials/compressible-tims/heatspring/ (accessed October 4, 2025).
[167] X. Wang, C. Lu, W. Rao, Liquid metal-based thermal interface materials with a high thermal conductivity for electronic cooling and bioheat-transfer applications, Appl. Therm. Eng. 192 (2021), https://doi.org/10.1016/j.applthermaleng.2021.116937.
[168] X.H. Yang, J. Liu, Advances in liquid metal science and technology in chip cooling and thermal management, Adv. Heat Transf. 50 (2018), https://doi.org/10.1016/bs.aiht.2018.07.002.
[169] N. Malu, D. Bora, S. Nakanekar, S. Tonapi, Thermal management of an IGBT module using two-phase cooling, in: Thermomechanical Phenomena in Electronic Systems -Proceedings of the Intersociety Conference, 2014. https://doi.org/10.1109/ITHERM.2014.6892401.
[170] S. Chen, Z. Deng, J. Liu, High performance liquid metal thermal interface materials, Nanotechnology 32 (2021), https://doi.org/10.1088/1361-6528/abcbc2.
[171] X.D. Zhang, J.Y. Gao, P.J. Zhang, J. Liu, Comparison on enhanced phase change heat transfer of low melting point metal melting using different heating methods, J. Enhanced Heat Transf. 26 (2019), https://doi.org/10.1615/JEnhHeatTransf.2018029198.
[172] X. Chen, J. Sun, J. Liang, R. Xing, J. Kong, Surface and interface engineering in gallium-based liquid metals, Adv. Funct. Mater. 36 (2026), https://doi.org/10.1002/adfm.202519697.
[173] Y. Yan, Y. Zhuang, H. Ouyang, J. Hao, X. Han, Experimental investigation on optimization of the performance of gallium-based liquid metal with high thermal conductivity as thermal interface material for efficient electronic cooling, Int. J. Heat Mass Transf. 226 (2024) 125455, https://doi.org/10.1016/j.ijheatmasstransfer.2024.125455.
[174] C.K. Roy, S. Bhavnani, M.C. Hamilton, R.W. Johnson, J.L. Nguyen, R.W. Knight, D.K. Harris, Investigation into the application of low melting temperature alloys as wet thermal interface materials, Int. J. Heat Mass Transf. 85 (2015), https://doi.org/10.1016/j.ijheatmasstransfer.2015.02.029.
[175] K. Huang, W. Qiu, M. Ou, X. Liu, Z. Liao, S. Chu, An anti-leakage liquid metal thermal interface material, RSC Adv. 10 (2020), https://doi.org/10.1039/d0ra02351e.
[176] J. Zhang, S. Yan, Q. An, T. Wu, L. Zou, Enhancing Bi-directional thermal conductivity: a novel tri-layer graphene-liquid metal composite for advanced thermal management, Compos. Commun. 55 (2025) 102319, https://doi.org/10.1016/j.coco.2025.102319.
[177] D. Wu, Z. Ning, Y. Zhu, R. Yuan, Evaluation of thermal and mechanical properties of Bi-In-Sn/WO_3 composites for efficient heat dissipation, Materials 17 (2024), https://doi.org/10.3390/ma17215315.
[178] Z. Lin, H. Liu, Q. Li, H. Liu, S. Chu, Y. Yang, G. Chu, High thermal conductivity liquid metal pad for heat dissipation in electronic devices, Appl. Phys. A Mater. Sci. Process. 124 (2018), https://doi.org/10.1007/s00339-018-1778-z.
[179] H. Wang, W. Xing, S. Chen, C. Song, M.D. Dickey, T. Deng, Liquid metal composites with enhanced thermal conductivity and stability using molecular thermal linker, Adv. Mater. 33 (2021) 2103104, https://doi.org/10.1002/adma.202103104.
[180] N. Si, Q. Yan, H. Zhang, Q. Li, J. Zhu, B. Huang, M. Wu, K. Yang, K. Wu, T. Cai, Y. Wang, J. Yu, N. Jiang, C. Xue, X. Hu, W. Dai, C.-T. Lin, Surface-metallized diamond/liquid metal composites through diamond size engineering as high-performance thermal interface materials, Surf. Interfaces 60 (2025) 105989, https://doi.org/10.1016/j.surfin.2025.105989.
[181] D. Shah, Liquid Metal Embedded Elastomers (LMEE) as Low-BLT Thermal Interface Materials, in: IMAPSource Proceedings 2024 (DPC), iMAPs, 2025. https://doi.org/10.4071/001c.129014.
[182] S. Mei, Y. Gao, Z. Deng, J. Liu, Thermally conductive and highly electrically resistive grease through homogeneously dispersing liquid metal droplets inside methyl silicone oil, J. Electron. Packag. 136 (2014), https://doi.org/10.1115/1.4026414.
[183] C.K. Roy, S. Bhavnani, M.C. Hamilton, R.W. Johnson, R.W. Knight, D.K. Harris, Thermal performance of low melting temperature alloys at the interface between dissimilar materials, Appl. Therm. Eng. 99 (2016), https://doi.org/10.1016/j.applthermaleng.2016.01.036.
[184] F. Hou, D. Yang, G.Q. Zhang, D. Liu, Research on heat dissipation of high heat flux multi-chip GaN-based white LED lamp, in: 2011 12th International Conference on Electronic Packaging Technology and High Density Packaging, 2011: pp. 1–5. https://doi.org/10.1109/ICEPT.2011.6067020.
[185] S. Kumar, Himanshi, J. Prakash, A. Verma, Suman, R. Jasrotia, A. Kandwal, R. Verma, S. Kumar Godara, M.A.M. Khan, S.M. Alshehri, J. Ahmed, A review on properties and environmental applications of graphene and its derivative-based composites, Catalysts 13 (2023) 111, https://doi.org/10.3390/catal13010111.
[186] J. Li, Y. Zhang, T. Liang, X. Bai, Y. Pang, X. Zeng, Q. Hu, W. Tu, Z. Ye, G. Du, Thermal interface materials with both high through-plane thermal conductivity and excellent elastic compliance, Chem. Mater. 33 (2021) 8926–8937.
[187] X. Zeng, L. Ren, R. Sun, Preparation and Properties of Thermal Interface Materials, in: Thermal Management Materials for Electronic Packaging: Preparation, Characterization, and Devices, 2024: pp. 211–255. https://doi.org/10.1002/9783527843121.ch7.
[188] Z. Zhang, R. Yang, Y. Wang, K. Xu, W. Dai, J. Zhang, M. Li, L. Li, Y. Guo, Y. Qin, B. Zhu, Y. Zhou, X. Wang, T. Cai, C.-T. Lin, K. Nishimura, H. Li, N. Jiang, J. Yu, Enhanced thermal conductivity and reduced thermal resistance in carbon fiber-based thermal interface materials with vertically aligned structure, J. Mater. Chem. A Mater. (2024), https://doi.org/10.1039/D4TA03924F.
[189] H. Ma, B. Gao, M. Wang, Z. Yuan, J. Shen, J. Zhao, Y. Feng, Strategies for enhancing thermal conductivity of polymer-based thermal interface materials: a review, J. Mater. Sci. 56 (2021), https://doi.org/10.1007/s10853-020-05279-x.
[190] J. Gao, Q. Yan, L. Lv, X. Tan, J. Ying, K. Yang, J. Yu, S. Du, Q. Wei, R. Xiang, Y. Yao, X. Zeng, R. Sun, C.P. Wong, N. Jiang, C. Te Lin, W. Dai, Lightweight thermal interface materials based on hierarchically strucntured graphene paper with superior through-plane thermal conductivity, Chem. Eng. J. 419 (2021), https://doi.org/10.1016/j.cej.2021.129609.
[191] T. Shahnaz, G. Hayder, M.A. Shah, M.Z. Ramli, N. Ismail, C.K. Hua, N.M. Zahari, N.H. Mardi, F.E. Selamat, N. Kabilmiharbi, H.A. Aziz, Graphene-based nanoarchitecture as a potent cushioning/filler in polymer composites and their applications, J. Mater. Res. Technol. 28 (2024) 2671–2698, https://doi.org/10.1016/j.jmrt.2023.12.108.
[192] X. Guo, S. Cheng, B. Yan, Y. Li, Y. Zhou, W. Cai, Y. Zhang, X. Zhang, Extraordinary thermal conductivity of polyvinyl alcohol composite by aligning densified carbon fiber via magnetic field, Nano Res. 16 (2023), https://doi.org/10.1007/s12274-022-5023-x.
[193] S. Guo, K.H. Martinsen, A. Nkansah, J. Chen, Z. Shen, M. Murugesan, H. Zhang, L. Almhem, A. Ahtonen, J. Chen, J. Liu, Characterization of a Novel Cost-efficient and Environmentally Friendly Graphene-enhanced Thermal Interface Material, in: 2023 24th European Microelectronics and Packaging Conference & Exhibition (EMPC), IEEE, 2023: pp. 1–4. https://doi.org/10.23919/EMPC55870.2023.10418385.
[194] J. Chen, X. Huang, B. Sun, P. Jiang, Highly thermally conductive yet electrically insulating polymer/boron nitride nanosheets nanocomposite films for improved thermal management capability, ACS Nano 13 (2019), https://doi.org/10.1021/acsnano.8b06290.
[195] C.-W. Nan, R. Birringer, D.R. Clarke, H. Gleiter, Effective thermal conductivity of particulate composites with interfacial thermal resistance, J. Appl. Phys. 81 (1997) 6692–6699, https://doi.org/10.1063/1.365209.
[196] A.S. Dmitriev, Hybrid graphene nanocomposites: thermal interface materials and functional energy materials, Graph. Prod Appl. (2020), https://doi.org/10.5772/intechopen.89631.
[197] F. Kargar, Z. Barani, R. Salgado, B. Debnath, J.S. Lewis, E. Aytan, R.K. Lake, A. A. Balandin, Thermal percolation threshold and thermal properties of composites with high loading of graphene and boron nitride fillers, ACS Appl. Mater. Interfaces 10 (2018) 37555–37565, https://doi.org/10.1021/acsami.8b16616.
[198] A. Ohayon-Lavi, M. Buzaglo, S. Ligati, S. Peretz-Damari, G. Shachar, N. Pinsk, M. Riskin, Y. Schatzberg, I. Genish, O. Regev, Compression-enhanced thermal conductivity of carbon loaded polymer composites, Carbon N. Y. 163 (2020), https://doi.org/10.1016/j.carbon.2020.03.026.
[199] A. Li, C. Zhang, Y.F. Zhang, Thermal conductivity of graphene-polymer composites: mechanisms, properties, and applications, Polymers (Basel) 9 (2017), https://doi.org/10.3390/polym9090437.
[200] Y. Xu, D.D.L. Chung, C. Mroz, Thermally conducting aluminum nitride polymer-matrix composites, Compos. Part A Appl. Sci. Manuf. 32 (2001), https://doi.org/10.1016/S1359-835X(01)00023-9.
[201] K. Zhan, Y. Chen, Z. Xiong, Y. Zhang, S. Ding, F. Zhen, Z. Liu, Q. Wei, M. Liu, B. Sun, H.-M. Cheng, L. Qiu, Low thermal contact resistance boron nitride nanosheets composites enabled by interfacial arc-like phonon bridge, Nat. Commun. 15 (2024) 2905, https://doi.org/10.1038/s41467-024-47147-1.
[202] C. Liu, W. Wu, Y. Wang, X. Liu, Q. Chen, S. Xia, Silver nanoparticle-enhanced three-dimensional boron nitride/reduced graphene oxide skeletons for improving thermal conductivity of polymer composites, ACS Appl. Polym. Mater. 3 (2021), https://doi.org/10.1021/acsapm.1c00210.
[203] M. Liu, S.W. Chiang, X. Chu, J. Li, L. Gan, Y. He, B. Li, F. Kang, H. Du, Polymer composites with enhanced thermal conductivity via oriented boron nitride and alumina hybrid fillers assisted by 3-D printing, Ceram. Int. 46 (2020), https://doi.org/10.1016/j.ceramint.2020.05.096.
[204] M. Shtein, R. Nadiv, M. Buzaglo, K. Kahil, O. Regev, Thermally conductive graphene-polymer composites: size, percolation, and synergy effects, Chem. Mater. 27 (2015) 2100–2106, https://doi.org/10.1021/cm504550e.
[205] Z. Gao, Y. Wang, B. Zhang, L. Liu, X. Liu, Enhanced thermal conductivity of high-density polyethylene composites with hybrid fillers of flaky and spherical boron nitride particles, Polymers (Basel) 16 (2024), https://doi.org/10.3390/polym16020268.
[206] Y. Zhou, Y. Wang, M. Li, Y. Qin, R. Yang, K. Xu, Y. Guo, L. Li, Z. Zhang, J. Zhang, B. Zhu, C.-T. Lin, Y. Xu, K. Nishimura, N. Jiang, J. Yu, Ultra-high thermal conductivity multifunctional composites with uniaxially oriented boron nitride sheets for future wireless charging technology, Adv. Compos. Hybrid Mater. 8 (2025) 237, https://doi.org/10.1007/s42114-025-01308-y.
[207] H. Niu, H. Guo, L. Kang, L. Ren, R. Lv, L. Liu, A. Bashir, S. Bai, Highly thermally conductive and soft thermal interface materials based on vertically oriented boron nitride film, Compos. B Eng. 272 (2024) 111219, https://doi.org/10.1016/j.compositesb.2024.111219.
[208] J. Li, X. Zhao, W. Wu, Z. Zhang, Y. Xian, Y. Lin, Y. Lu, L. Zhang, Advanced flexible rGO-BN natural rubber films with high thermal conductivity for improved thermal management capability, Carbon N. Y. 162 (2020), https://doi.org/10.1016/j.carbon.2020.02.012.
[209] Y. Zhang, Y.J. Heo, Y.R. Son, I. In, K.H. An, B.J. Kim, S.J. Park, Recent advanced thermal interfacial materials: a review of conducting mechanisms and parameters of carbon materials, Carbon N. Y. 142 (2019), https://doi.org/10.1016/j.carbon.2018.10.077.
[210] L. Fan, B. Su, J. Qu, C.P. Wong, Electrical and thermal conductivities of polymer composites containing nano-sized particles, Proc. – Electron. Components Technol. Conf. (2004).

[211] Y. Li, X. Liao, X. Guo, S. Cheng, R. Huang, Y. Zhou, W. Cai, Y. Zhang, X. Zhang, Improving thermal conductivity of epoxy-based composites by diamond-graphene binary fillers, Diam. Relat. Mater. 126 (2022) 109141, https://doi.org/10.1016/j.diamond.2022.109141.
[212] P. Corporation, PGS (Pyrolytic Graphite Sheet) — Technical Data Sheet, 2021. https://industrial.panasonic.com/cdbs/www-data/pdf/AYA0000/AYA0000C27.pdf.
[213] A. Nylander, J. Hansson, T. Nilsson, L. Ye, Y. Fu, J. Liu, Degradation of carbon nanotube array thermal interface materials through thermal aging: effects of bonding, array height, and catalyst oxidation, ACS Appl. Mater. Interfaces 13 (2021) 30992–31000, https://doi.org/10.1021/acsami.1c05685.
[214] X. Zeng, J. Sun, Y. Yao, R. Sun, J. Bin Xu, C.P. Wong, A combination of boron nitride nanotubes and cellulose nanofibers for the preparation of a nanocomposite with high thermal conductivity, ACS Nano 11 (2017), https://doi.org/10.1021/acsnano.7b02359.
[215] E. Pop, D. Mann, Q. Wang, K. Goodson, H. Dai, Thermal conductance of an individual single-wall carbon nanotube above room temperature, Nano Lett. 6 (2006), https://doi.org/10.1021/nl052145f.
[216] S. Harish, D. Orejon, Y. Takata, M. Kohno, Thermal conductivity enhancement of lauric acid phase change nanocomposite with graphene nanoplatelets, Appl. Therm. Eng. 80 (2015), https://doi.org/10.1016/j.applthermaleng.2015.01.056.
[217] M.J. Biercuk, M.C. Llaguno, M. Radosavljevic, J.K. Hyun, A.T. Johnson, J. E. Fischer, Carbon nanotube composites for thermal management, Appl. Phys. Lett. 80 (2002) 2767–2769, https://doi.org/10.1063/1.1469696.
[218] Y. Pei, H. Zhong, M. Wang, P. Zhang, Y. Zhao, Effect of contact pressure on the performance of carbon nanotube arrays thermal interface material, Nanomaterials 8 (2018), https://doi.org/10.3390/nano8090732.
[219] V. Ghai, A.A. Mishra, E. Huang, R. Ngaloy, S.P. Dash, A. Matic, R. Kádár, Halbach array induced magnetic field alignment in boron nitride nanocomposites, Adv. Sci. 12 (2025) 2408532, https://doi.org/10.1002/advs.202408532.
[220] M. He, L. Zhang, K. Ruan, J. Zhang, H. Zhang, P. Lv, Y. Guo, X. Shi, H. Guo, J. Kong, J. Gu, Functionalized aluminum nitride for improving hydrolysis resistances of highly thermally conductive polysiloxane composites, Nanomicro Lett. 17 (2025) 134, https://doi.org/10.1007/s40820-025-01669-5.
[221] R. Qian, J. Yu, C. Wu, X. Zhai, P. Jiang, Alumina-coated graphene sheet hybrids for electrically insulating polymer composites with high thermal conductivity, RSC Adv. 3 (2013) 17373–17379, https://doi.org/10.1039/C3RA42104J.
[222] M. Wang, H. Chen, W. Lin, Z. Li, Q. Li, M. Chen, F. Meng, Y. Xing, Y. Yao, C. Wong, Q. Li, Crack-free and scalable transfer of carbon nanotube arrays into flexible and highly thermal conductive composite film, ACS Appl. Mater. Interfaces 6 (2014) 539–544, https://doi.org/10.1021/am404594m.
[223] A. Tarhini, A.R. Tehrani-Bagha, Advances in preparation methods and conductivity properties of graphene-based polymer composites, Appl. Compos. Mater. 30 (2023) 1737–1762, https://doi.org/10.1007/s10443-023-10145-5.
[224] F. An, X. Li, P. Min, P. Liu, Z.-G. Jiang, Z.-Z. Yu, Vertically aligned high-quality graphene foams for anisotropically conductive polymer composites with ultrahigh through-plane thermal conductivities, ACS Appl. Mater. Interfaces 10 (2018) 17383–17392, https://doi.org/10.1021/acsami.8b04230.
[225] W. Dai, L. Le, T. Ma, W. Xiangze, J. Ying, Y. Qingwei, X. Tan, J. Gao, C. Xue, J. Yu, Y. Yao, Q. Wei, R. Sun, Y. Wang, T. Liu, T. Chen, R. Xiang, N. Jiang, Q. Xue, C.-T. Lin, Multiscale structural modulation of anisotropic graphene framework for polymer composites achieving highly efficient thermal energy management, Adv. Sci. 8 (2021), https://doi.org/10.1002/advs.202003734.
[226] J. Yue, S. Hu, B. Xu, R. Chen, L. Xiong, R. Guo, Y. Li, L.-L. Nian, J. Shiomi, B. Zheng, Unraveling the mechanisms of thermal boundary conductance at the graphene-silicon interface: insights from ballistic, diffusive, and localized phonon transport regimes, Phys. Rev. B 109 (2024) 115302.
[227] R. Mohanraman, P. Steiner, C. Kocabas, I.A. Kinloch, M.A. Bissett, Synergistic improvement in the thermal conductivity of hybrid boron nitride nanotube/nanosheet epoxy composites, ACS Appl. Nano Mater. 7 (2024) 13142–13146, https://doi.org/10.1021/acsanm.4c01646.
[228] J.H. Kim, T.V. Pham, J.H. Hwang, C.S. Kim, M.J. Kim, Boron nitride nanotubes: synthesis and applications, Nano Converg. 5 (2018) 17, https://doi.org/10.1186/s40580-018-0149-y.
[229] M.B. Jakubinek, J.F. Niven, M.B. Johnson, B. Ashrafi, K.S. Kim, B. Simard, M. A. White, Thermal conductivity of bulk boron nitride nanotube sheets and their epoxy-impregnated composites, Physica Status Solidi (a) 213 (2016) 2237–2242, https://doi.org/10.1002/pssa.201533010.
[230] Y. Martinez-Rubi, B. Ashrafi, M.B. Jakubinek, S. Zou, K.S. Kim, H. Cho, B. Simard, Nanocomposite fabrics with high content of boron nitride nanotubes for tough and multifunctional composites, J. Mater. Res. 37 (2022) 4553–4565, https://doi.org/10.1557/s43578-022-00707-x.
[231] T. Lim, J. Yoo, H. Park, O. Alduhaish, I. Rabani, Y.-S. Seo, Integrating boron nitride nanotubes into functionalized boron nitride/epoxy composites enhances thermal conductivity and other properties, ACS Appl. Polym. Mater. 6 (2024) 9477–9487, https://doi.org/10.1021/acsapm.4c01099.
[232] V. Goyal, A.A. Balandin, Thermal properties of the hybrid graphene-metal nano-micro-composites: applications in thermal interface materials, Appl. Phys. Lett. 100 (2012), https://doi.org/10.1063/1.3687173.
[233] K.M.F. Shahil, A.A. Balandin, Thermal properties of graphene and multilayer graphene: applications in thermal interface materials, Solid State Commun. 152 (2012), https://doi.org/10.1016/j.ssc.2012.04.034.
[234] P. Zhang, J. Zeng, S. Zhai, Y. Xian, D. Yang, Q. Li, Thermal properties of graphene filled polymer composite thermal interface materials, Macromol. Mater. Eng. 302 (2017), https://doi.org/10.1002/mame.201700068.
[235] H. Zhang, Y. Lin, D. Zhang, W. Wang, Y. Xing, J. Lin, H. Hong, C. Li, Graphene nanosheet/silicone composite with enhanced thermal conductivity and its application in heat dissipation of high-power light-emitting diodes, Curr. Appl Phys. 16 (2016), https://doi.org/10.1016/j.cap.2016.10.004.
[236] X. Wang, Z. Pu, Y. Yang, B. Wei, S. Yang, Ultra-high thermal conductive epoxy-based copper/graphite nanoplatelets materials for heat management application, Compos. Sci. Technol. 224 (2022) 109454, https://doi.org/10.1016/j.compscitech.2022.109454.
[237] S. Choi, H. Im, J. Kim, Flexible and high thermal conductivity thin films based on polymer: aminated multi-walled carbon nanotubes/micro-aluminum nitride hybrid composites, Compos. Part A Appl. Sci. Manuf. 43 (2012) 1860–1868, https://doi.org/10.1016/j.compositesa.2012.06.009.
[238] R.C. Campbell, S.E. Smith, R.L. Dietz, Measurements of adhesive bondline effective thermal conductivity and thermal resistance using the laser flash method, Annu. IEEE Semicond. Therm. Meas. Manag. Symp. (1999), https://doi.org/10.1109/stherm.1999.762433.
[239] S. Wang, Y. Cheng, R. Wang, J. Sun, L. Gao, Highly thermal conductive copper nanowire composites with ultralow loading: toward applications as thermal interface materials, ACS Appl. Mater. Interfaces (2014), https://doi.org/10.1021/am500009p.
[240] J. Gu, X. Yang, Z. Lv, N. Li, C. Liang, Q. Zhang, Functionalized graphite nanoplatelets/epoxy resin nanocomposites with high thermal conductivity, Int. J. Heat Mass Transf. 92 (2016), https://doi.org/10.1016/j.ijheatmasstransfer.2015.08.081.
[241] W. Guo, G. Chen, Fabrication of graphene/epoxy resin composites with much enhanced thermal conductivity via ball milling technique, J. Appl. Polym. Sci. 131 (2014), https://doi.org/10.1002/app.40565.
[242] W. Zhou, S. Qi, Q. An, H. Zhao, N. Liu, Thermal conductivity of boron nitride reinforced polyethylene composites, Mater. Res. Bull. 42 (2007), https://doi.org/10.1016/j.materresbull.2006.11.047.
[243] J. Gu, Q. Zhang, J. Dang, C. Xie, Thermal conductivity epoxy resin composites filled with boron nitride, Polym. Adv. Technol. 23 (2012), https://doi.org/10.1002/pat.2063.
[244] E.S. Lee, S.M. Lee, D.J. Shanefield, W.R. Cannon, Enhanced thermal conductivity of polymer matrix composite via high solids loading of aluminum nitride in epoxy resin, J. Am. Ceram. Soc. 91 (2008), https://doi.org/10.1111/j.1551-2916.2008.02247.x.
[245] S.Y. Pak, H.M. Kim, S.Y. Kim, J.R. Youn, Synergistic improvement of thermal conductivity of thermoplastic composites with mixed boron nitride and multi-walled carbon nanotube fillers, Carbon N. Y. 50 (2012), https://doi.org/10.1016/j.carbon.2012.06.009.
[246] D. Liang, P. Ren, F. Ren, Y. Jin, J. Wang, C. Feng, Q. Duan, Synergetic enhancement of thermal conductivity by constructing BN and AlN hybrid network in epoxy matrix, J. Polym. Res. 27 (2020), https://doi.org/10.1007/s10965-020-02193-3.
[247] M. Kozako, Y. Okazaki, M. Hikita, T. Tanaka, Preparation and evaluation of epoxy composite insulating materials toward high thermal conductivity, in: Proceedings of the 2010 IEEE International Conference on Solid Dielectrics, ICSD 2010, 2010. https://doi.org/10.1109/ICSD.2010.5568250.
[248] V.D. Mai, D. Il Lee, J.H. Park, D.S. Lee, Rheological properties and thermal conductivity of epoxy resins filled with a mixture of alumina and boron nitride, Polymers (Basel) 11 (2019), https://doi.org/10.3390/polym11040597.
[249] C. Lei, Y. Zhang, D. Liu, X. Xu, K. Wu, Q. Fu, Highly thermo-conductive yet electrically insulating material with perpendicularly engineered assembly of boron nitride nanosheets, Compos. Sci. Technol. 214 (2021), https://doi.org/10.1016/j.compscitech.2021.108995.
[250] E.O. Maina, I. El Hajj, R. Li, A. Teruzzi, K. Dembélé, A.H. Denawi, D. Dragoe, H. Vach, F.Z. Bouanis, Scalable fabrication of a Ti3C2Tx-MXene@graphene-based humidity sensor via MILD etching and interfacial self-assembly, Mater. Today Nano (2026) 100819, https://doi.org/10.1016/j.mtnano.2026.100819.
[251] X. Li, D. Zou, L. Tong, M. Li, Y. Dong, S. Xu, Q. Wang, K. Wang, Bio-inspired MXene/graphene oxide-based nanocomposites with enhanced interfacial self-healing effects and multifunctional integration, Chem. Eng. J. 513 (2025) 162857, https://doi.org/10.1016/j.cej.2025.162857.
[252] M.S. Mohtasim, B.K. Das, MXene based composite phase change materials for thermal energy storage applications: featuring bio-mimic approaches, Renew. Sustain. Energy Rev. 207 (2025) 114952, https://doi.org/10.1016/j.rser.2024.114952.
[253] J.L. Stoll, M. Paul, L. Pritchett, A. Snover, L. Woods, S. Antony Jose, P.L. Menezes, Tribology of MXene materials: advances, challenges, and future directions, Materials 18 (2025) 4767, https://doi.org/10.3390/ma18204767.
[254] A. Adhami, M. Mozafari, M. Soroush, MXene-based stimuli-responsive and autonomous intelligent materials, Commun. Mater. 7 (2026) 36, https://doi.org/10.1038/s43246-026-01074-4.
[255] M. Akter, H.R. Anik, M.K.H. Chowdhury, S.M.M. Hasan, I. Hossain, A. Chakrabortty, Md. Nahid-Ull-Islam, M. Mahfuzur Rahman, Recent advances in MXene-based 3D-printed smart textiles: a review on functional properties, fabrication processes, and applications, Adv. Eng. Mater. 27 (2025), https://doi.org/10.1002/adem.202501909.
[256] R. Khazaka, R. Hanna, Y. Avenas, S. Azzopardi, Analysis of power modules including phase change materials in the top interconnection of semiconductor devices, Electron. Mater. 5 (2024) 204–220, https://doi.org/10.3390/electronicmat5040014.
[257] M. Li, S. Han, C. Dan, T. Wu, F. You, X. Jiang, Y. Wu, Z.-M. Dang, Boron nitride-polymer composites with high thermal conductivity: preparation,

functionalization strategy and innovative structural regulation, Small 21 (2025) 2412447, https://doi.org/10.1002/smll.202412447.
[258] B. Singh, J. Han, M. Meziani, L. Cao, S. Yerra, J. Collins, S. Dumra, S. Yaping, Polymeric nanocomposites of boron nitride nanosheets for enhanced directional or isotropic thermal transport performance, Nanomaterials 14 (2024) 1259, https://doi.org/10.3390/nano14151259.
[259] Y. Sun, L. Wang, Y. Ni, H. Zhang, X. Cui, J. Li, Y. Zhu, J. Liu, S. Zhang, Y. Chen, M. Li, 3D printing of thermosets with diverse rheological and functional applicabilities, Nat. Commun. 14 (2023) 245, https://doi.org/10.1038/s41467-023-35929-y.
[260] Materials Characterization Services, ASTM D5470 – Standard Test Method for Thermal Transmission Properties of Thermally Conductive Electrical Insulation Materials, (2025). \url{https://mat-cs.com/astm-d5470/ (accessed October 6, 2025).
[261] CreeLED, JESD51-14 Thermal Resistance Calculation Method (Application Note), (2022). https://downloads.cree-led.com/files/da/x/JESD51-14-Thermal-Resistance-Calculation.pdf (accessed October 6, 2025).